UCRL-17095

University of California

Ernest O. Lawrence Radiation Laboratory

EFFECT OF HIGH PRESSURE ON THE PROPERTIES OF SOME METALS

TWO-WEEK LOAN COPY

This is a Library Circulating Copy which may be borrowed for two weeks. For a personal retention copy, call Tech. Info. Division, Ext. 5545

Berkeley, California

DISCLAIMER

This document was prepared as an account of work sponsored by the United States Government. While this document is believed to contain correct information, neither the United States Government nor any agency thereof, nor the Regents of the University of California, nor any of their employees, makes any warranty, express or implied, or assumes any legal responsibility for the accuracy, completeness, or usefulness of any information, apparatus, product, or process disclosed, or represents that its use would not infringe privately owned rights. Reference herein to any specific commercial product, process, or service by its trade name, trademark, manufacturer, or otherwise, does not necessarily constitute or imply its endorsement, recommendation, or favoring by the United States Government or any agency thereof, or the Regents of the University of California. The views and opinions of authors expressed herein do not necessarily state or reflect those of the United States Government or any agency thereof or the Regents of the University of California.

UCRL-17095

UNIVERSITY OF CALIFORNIA

Lawrence Radiation Laboratory
Berkeley, California

AEC Contract No. W-7405-eng-48

EFFECT OF HIGH PRESSURE ON THE PROPERTIES OF SOME METALS

Donald Louis Raimondi

(Ph. D. Thesis)

September 1966

TABLE OF CONTENTS

ABSTRACT . . . v

I An Experimental Equation of State for Aluminum . . . 1

A. Introduction . . . 1

B. Theory . . . 3

1. General . . . 3

2. Resistivity of Simple Metals . . . 5

C. Experimental . . . 16

D. Results . . . 24

E. Discussion . . . 36

F. Conclusions . . . 41

II Effect of Pressure on the Mossbauer Spectrum of Fe^{57} in Iron and Nickel Metal . . . 42

A. Introduction . . . 42

B. Theory . . . 43

1. General . . . 43

2. Effect of Pressure on the Mossbauer Effect . . . 53

C. Experimental . . . 56

1. General . . . 56

2. Mossbauer Spectrometer . . . 59

3. Data Analysis . . . 66

D. Iron Experiment . . . 71

1. Introduction . . . 71

2. Experimental . . . 77

3. Results and Discussion . . . 77

4. Conclusions . . . 81

E. Nickel Experiment . . . 82

1. Introduction . . . 82

2. Experimental . . . 86

3. Discussion . . . 90

4. Conclusions . . . 93

Acknowledgments . . . 94

References . . . 95

EFFECT OF HIGH PRESSURE ON THE PROPERTIES OF SOME METALS

Donald Louis Raimondi

Inorganic Materials Research Division,
Lawrence Radiation Laboratory,
Department of Chemistry
University of California, Berkeley, California

ABSTRACT

September 1966

An equation of state for aluminum to the Debye approximation has been obtained from the determination of the Debye temperature, Θ, as a function of pressure from 0 to 135 kbars. The variation was determined by use of the Bloch-Grüneisen equation in fitting experimental resistance-temperature data at various pressures. The zero pressure thermodynamic properties of aluminum calculated from the equation of state agree quite well with the corresponding observed quantities. It is found that the Grüneisen ratio, $-d\ln\Theta/d\ln V$, is a linear function of volume at pressures above 40 kbars. An analytical expression which approximates the observed volume dependence of the Debye temperature is given by,

$$\Theta = 395\ e^{-1.78\Delta V/V_0} .$$

The effect of high pressure on the Mössbauer spectrum of Fe^{57} in iron was studied to a pressure of 140 kbars with particular interest in the transition of α-iron to the hcp phase. Because of the low intensity of the observed Mössbauer lines, the results are qualitative. A current-pulse technique was applied to the iron at pressures of 120 kbars and above, but a sharp transition was not observed. It was found that after decompression from 140 kbars to 120 kbars, the transformation of hcp-iron to α-iron could be followed kinetically by measuring the decrease in intensity of a strong single line characteristic of the hcp-iron and correspondingly, the increase in the intensity of the normal six line

spectrum of α-iron. The estimated rate constant for the transformation of hcp-iron to α-iron at 120 kbars and 298°K is 0.012 hr^{-1}.

In order to better understand the interaction of the ferromagnetic host with an impurity atom in a dilute alloy, the Mössbauer spectrum of Fe^{57} in nickel metal was studied to 80 kbars. A peak in the internal field at the Fe^{57} nucleus was observed at 10 kbars, followed by a slow decrease up to 80 kbars. The initial increase of the internal field with pressure is given by

$$\frac{d\ln H}{dP} = 10.2 \times 10^{-4} \text{ kbar}^{-1} .$$

The change in the isomer shift over the entire pressure range is given by

$$\frac{d(IS)}{dP} = -4.15\times10^{-5} \text{ cm sec}^{-1}\text{kbar}^{-1}.$$

These results are discussed as they relate to other pressure studies on the properties of pure nickel and iron.

I. AN EXPERIMENTAL EQUATION OF STATE FOR ALUMINUM

A. Introduction

An accurate determination of the equation of state of a substance is probably the most basic physical problem confronting the experimentalist today. As theories are advanced it becomes ever more necessary to complement them with accurate data with which they may be tested. In addition, precise knowledge of the behavior of materials under the extremes of temperature and pressure is essential in complex engineering problems. Despite the importance of this problem, relatively little equation of state data are available for solids.

Until the recent development of x-ray diffraction methods for the determination of the pressure-volume-temperature relationships of solids,[1] the shock technique was the most widely applicable technique for the determination of equations of state. The reliability of shock measurements decreases rapidly below 100 kbars for most materials and thus most of the available equation of state data have been obtained above 100 kbars.[2] It is certainly desirable to complement the shock data with direct determinations from 1 atmosphere to a pressure above 100 kbars using static high pressure techniques.

Several static techniques are available for the determination of an equation of state. Piston displacement methods are generally applicable to materials that show large volume changes with pressure and have thus been applied to studies of the alkali metals and solid rare gases.[3] Elastic constant determinations yield very precise results but to date the experimental difficulties above 10-15 kbars have not been mastered. Anderson[4] has performed the most comprehensive investigation of this

problem in his work on silica. X-ray diffraction methods promise to provide an easily applied technique, but have not been used to date for equation of state investigations. Because high pressure vessels are so massive, the normal methods of heat capacity measurements are not applicable. Calorimetry has been applied only to solid helium[5] and solid hydrogen[6] to a few kilobars. A new high pressure heat capacity technique developed in this laboratory by Stark and Jura[7] promises to open up a new field of research possibilities for the determination of equations of state. This technique consists of measuring the heat capacity of metallic wire samples under high pressure by a current pulse technique similar to that used by Wallace et al.[8] at atmospheric pressure.

In the present work, the heat capacity and thermodynamic properties of aluminum are determined to the Debye approximation. This is accomplished by determining the Debye temperature of aluminum by application of the Bloch-Grüneisen equation to resistance temperature measurements on aluminum. The Debye temperature of aluminum increases from 395° at 1 atmosphere to 485° at 135 kbars.

B. Theory

1. General

The equation of state of a solid

$$P = P(V,T) \quad , \tag{I-1}$$

may be derived from the Helmholtz free energy A, where A is defined by the thermodynamic identity

$$A = E - TS, \tag{I-2}$$

and the pressure by

$$P = -\left(\frac{\partial A}{\partial V}\right)_T \quad . \tag{I-3}$$

Now we may write approximately

$$A = E_0(V) + A^*(T,V) \quad , \tag{I-4}$$

where $E_0(V)$ is the internal energy at 0°K and $A^*(T,V)$ is the contribution of the lattice vibrations to the free energy. The expression for the pressure is then written

$$P(V,T) = P_0(V) + P^*(V,T) \quad . \tag{I-5}$$

$P_0(V)$ is the pressure needed to obtain the volume V at absolute zero, and $P^*(V,T)$ is an additional thermal pressure due to lattice vibrations. In general, these terms are very difficult to calculate from first principles. Bernardes and Swenson[9] review the theory and recent progress in the calculation of the equation of state. We must know the vibrational spectrum of the lattice and its variation with volume. The simple assumption that all the vibrational frequencies are changed in the same manner by a change in volume leads to the Mie-Grüneisen equation of state[10]

$$P = -\frac{dE_0}{dV} + \frac{\gamma}{V} E^*(V,T) \ , \tag{I-6}$$

where γ is the Grüneisen ratio describing the volume variation of the vibrational frequencies and defined by

$$\gamma = \frac{d\ln\nu_i}{d\ln V} . \qquad \text{(I-7)}$$

$E^*(V,T)$, the thermal energy, is given by

$$E^*(V,T) = \sum_i \frac{h\nu_i}{e^{h\nu_i/kT}-1} . \qquad \text{(I-8)}$$

Differentiation of Eq. (I-6) yields an expression for the Grüneisen ratio in terms of measurable thermodynamic quantities. This expression

$$\gamma = \frac{-(\partial V/\partial T)_P V}{C_V(\partial V/\partial P)_T} = \frac{\alpha V}{\beta C_V} \qquad \text{(I-9)}$$

is known as Grüneisen's law. It allows one to evaluate γ from known values of the heat capacity (C_V), thermal expansion $\left(\frac{1}{V}(\partial V/\partial T)_P\right)$, and compressibility $\left(-\frac{1}{V}(\partial V/\partial P)_T\right)$. Barron[11,12] has extended the Born-von-Kármán theory to an essentially exact calculation of the Gruneisen ratio for a few simple models. His results show that the Grüneisen law is invalid at low temperature, but applies quite well above 0.3Θ.

A specific case of the Mie-Grüneisen equation of state may be derived if a model is assumed to describe the thermal energy. Assuming a Debye model for the lattice spectrum, we have the Debye equation of state

$$P = -\frac{dE_0}{dV} + \frac{\gamma}{V}(E-E_0) , \qquad \text{(I-10)}$$

where $(E-E_0)$ is given by the appropriate Debye integral and γ is now given by

$$\gamma = -\frac{d\ln\Theta}{d\ln V} , \qquad \text{(I-11)}$$

where Θ is the Debye temperature of the solid. Equation (I-10) is then a single parameter equation of state. A knowledge of the volume dependence of the Debye temperature need only be combined with a single pressure-volume isotherm to completely specify the equation of state of the system.

Ordinary methods for the determination of Debye temperatures such as the use of heat capacity and elastic constant data do not apply since a knowledge of these data is in itself a determination of the equation

of state. An independent technique is the determination of the Debye temperature from resistance-temperature data, by application of the Bloch-Grüneisen theory[13,14] of resistances. In order to understand the application of this theory in its relationship to equation of state investigations, a qualitative discussion of the resistivity and the effect of pressure on the resistivity of simple metals follows. For a more complete description of the problem see Ziman's Principles of the Theory of Solids.[15]

2. Resistivity of Simple Metals

Although there has been a qualitative understanding of the electrical resistivity of metals for some time, no precise quantitative theory has been developed which can explain the electrical properties of even the simplest metals. Ziman[16] points out that at present theoreticians are just beginning to understand how to calculate the electronic transport properties of very simple metals at their normal volume.

According to the classical model of an electron gas, electrons move randomly with a Maxwell-Boltzmann distribution of velocities. On applying an electrical field $\vec{E}$ the electrons acquire a drift velocity, limited by scattering processes, which provides a current density $\vec{j}$. Applying simple kinetic theory, the electrical resistivity is then

$$\rho = \frac{\vec{E}}{\vec{j}} = \frac{m}{ne^2\tau} \quad , \qquad \text{(I-12)}$$

where n is the number of electrons per unit volume, τ is the electron relaxation time or average time between collisions, and e and m are the electronic charge and mass, respectively. This is also written in terms of a mean free path, l,

$$\rho = \frac{mv}{ne^2 l} \quad , \qquad \text{(I-13)}$$

where v is the mean velocity of the electrons. Replacing the classical electron gas by the Fermi gas, one modification is required. Since only electrons at the top of the Fermi distribution may be accelerated in an electric field, the value of v is approximately constant and equal to v_F, corresponding to the Fermi energy, W_F. Thus, changes in electrical resistivity with temperature depend primarily on changes in the mean free path.

The mean free path of electrons is limited by scattering processes. The two main types of electron scattering for simple metals are phonon and impurity scattering. The expression "simple" is used in general to exclude transition metals. The electrical resistivity of transition metals is complicated by scattering into the unfilled d-band. To a good approximation phonon and impurity scattering are independent and their associated resistivity contributions may be added. This is known as Matheissen's rule.[17]

a. Phonon scattering. At low temperatures ($T \ll \Theta$) the interaction between an electron and a phonon is weak. In other words, little energy is exchanged in an electron-phonon collision and the electron is scattered through a small angle. This is seen by considering a single collision and comparing the relative magnitudes of the electron and phonon momenta, p, or their respective k vectors where

$$k = \frac{2\pi}{\lambda} = \frac{2\pi p}{\hbar} \quad . \qquad \text{(I-14)}$$

From the Debye theory of specific heats we have for $T < \Theta$ that the dominant lattice wavelength, λ, is of the order of $(2a\Theta/T)$, where a is the lattice constant. For simple "one electron metals" where the conduction band is half-full the value of the k-vector at the Fermi surface

is approximately π/a. Thus, the average angle ϕ through which an electron is scattered by a phonon is given by

$$\phi \approx \frac{k(\text{phonon})}{k(\text{electron})} \approx T/\Theta \ . \qquad \text{(I-15)}$$

Now, from a statistical treatment the effective mean free path, l_{eff}, associated with the drift of electrons in an electric field is $1/(1-\cos\phi)$ times the average path l_0 between small angle scattering collisions when there is no applied electric field. For $T \ll \Theta$, this may be written

$$l_{eff} = \frac{l_0}{(1 - \cos\phi)} \propto \frac{l_0}{T^2} \qquad \text{(I-16)}$$

If each electron-phonon scattering process is considered to be a purely random scattering process the mean free path of electrons between small angle scattering collisions is then inversely proportional to the density of phonons. At low temperatures the phonon density is proportional to T^3 and thus l_{eff} is given by

$$\rho_{phonon} \propto \frac{1}{l_{eff}} \propto T^5 (T \ll \Theta). \qquad \text{(I-17)}$$

Now as the temperature increases the scattering angle increases and the effective mean free path of electrons depends only on the phonon density, which is proportional to the absolute temperature. Thus, the resistivity is given simply by

$$\rho_{phonon} \propto T \ (T \geq \Theta). \qquad \text{(I-18)}$$

The linear and fifth power temperature dependency of the resistivity at the high and low temperature limits are well known experimentally. The "T^5 law" is a characteristic quantum effect comparable with the T^3

law in the theory of specific heats.

Bloch[13] and Grüneisen[14] have independently derived a theoretical expression for the resistivity of simple metals. This equation assumes 1) a monovalent metal with a spherical Fermi surface, 2) a simplified mechanism for the scattering processes, and 3) a Debye model with temperature parameter, Θ, to describe the vibrational spectrum. It is called the Bloch-Gruneisen law and is written

$$\rho_{phonon} = A \frac{T^5}{\Theta^6} \int_0^{\Theta/T} \frac{Z^5 dZ}{(e^Z-1)(1-e^Z)} \cdots \qquad \text{(I-19)}$$

The parameter A contains volume dependent terms characteristic of the metal such as the Fermi energy, effective mass of the electrons, and a scattering parameter. The Bloch-Grüneisen law reduces to

$$\rho_{phonon} = B \frac{T^5}{\Theta^6} \quad \text{for } T \ll \Theta/T \qquad \text{(I-20)}$$

and to

$$\rho_{phonon} = C \frac{T}{\Theta^2} \quad \text{for } T \geq \Theta \quad . \qquad \text{(I-21)}$$

In actual practice, the absolute values of the resistance are not accurately given by Eq. (I-19), but the relative resistances as a function of temperature derived from this equation are in excellent agreement with those obtained from experiment. An often reproduced graph of the reduced resistivity of a number of metals versus reduced temperature, T/Θ, is illustrated in Fig. I-1. The optimum value of the Debye temperature to be used here may differ somewhat from the value deduced from specific heats. Table I-I compares Debye Θ's determined from specific heat data near room temperature with those determined from resistivity data for a few metals.

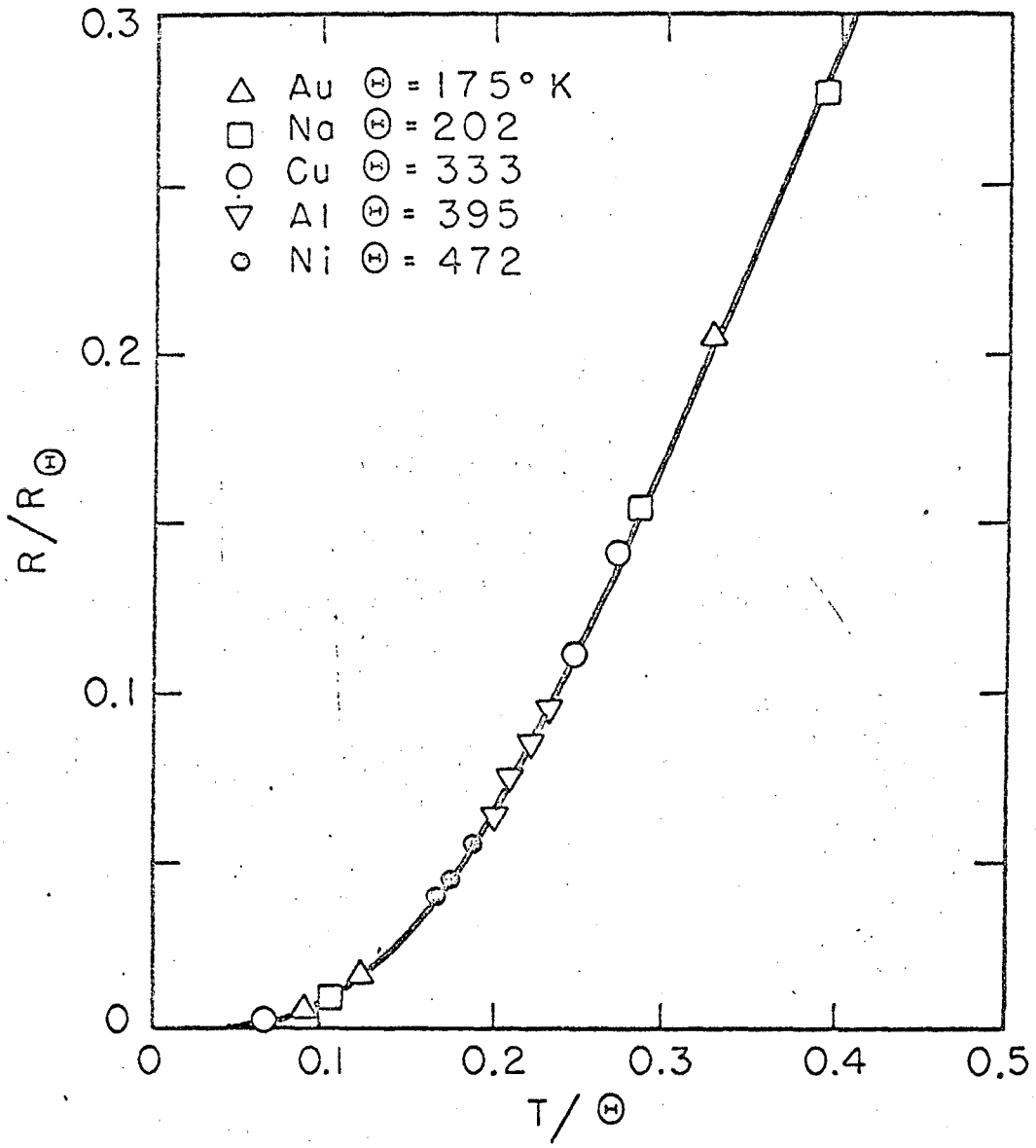

MUB-12683

Fig. I-1 Temperature variation of resistivity of various metals compared with the Bloch-Grüneisen equation (after Bardeen[18]).

Table I.I Debye temperatures determined by resistivity, Θ_R, and specific heats, Θ_D. (Ref. 19)

Metal	Θ_R	Θ_D
Li	363	352
Na	205	157
K	116	100
Rb	58	59
Cs	45	43
Al	395	398
Cu	333	342
Ag	223	228
Au	175	165
Sn	210	200
Pt	235	234
Pb	89	87

b. Impurity scattering. The presence of impurities provide static scattering centers which limit the mean free path of electrons to a constant value at very low temperatures. The temperature at which the impurity or residual resistance becomes appreciable with respect to the total resistance is dependent on the concentration and nature of the impurity atoms and on the specimen history. Mechanical deformation and thermal treatment may have a large effect on the residual resistance. Usually impurity effects are not important above a temperature of $\Theta/30$ for reasonably pure specimens (> 99%). Many metals exhibit a resistivity minimum at very low temperatures ($\sim 4^\circ$K).[20] This phenomena has received a great deal of attention, but to date there has been no satisfactory explanation, although it appears to be associated with impurities.[21]

c. Effect of pressure on the electrical resistivity. To further understand the application of the bloch-Grüneisen theory to metals at high pressures, the effect of pressure on the electrical resistivity is discussed. Pressure effects are divided into four categories. First, there is the change in the interaction of the conduction electrons and the lattice as a result of the lattice stiffening. Second, there is a change in the Fermi energy with pressure. Third, there is the possible appearance of new, more dense, crystallographic forms, and fourth, there are changes in the band structure of the metal arising from changes in overlap between various bands or from more radical changes in the electronic structure of the atoms.

Crystallographic transitions have allowed experimenters to use resistance measurements as a convenient tool in determining phase diagrams. Changes in band structure becomes very important in the consideration of

very compressible metals and those with complicated band structures. This is evidenced by the unusual behavior of some of the alkali metals[22] and the transformation of bismuth to a semiconducting state under pressure.[23]

But for most metals the primary cause of the change in the resistivity with pressure is the change of the electron-phonon interaction. Assuming the lattice resistivity is given by Eq. (I-21) in the high temperature limit, the variation of the resistance with volume is given to a first approximation by

$$\frac{d\ln R}{d\ln V} = -2\,\frac{d\ln\Theta}{d\ln V} = 2\gamma \quad , \qquad \text{(I-22)}$$

where γ is the Grüneisen ratio. Since γ is positive, the resistance decreases with decrease in volume or increase in pressure. This is generally the behavior of most metals. It is understood in simple terms, by considering that the increase in pressure increases the maximum allowable frequency of the atoms. Since there are only 3N possible modes, there are fewer modes excited at any given temperature. In the high temperature limit ($T \geq \Theta$) the resistivity is proportional to the density of phonons and thus decreases with pressure. Lennsen and Michels[24] considered the volume dependence of the resistance somewhat more elaborately and found

$$\frac{d\ln R}{d\ln V} = 2\gamma + \frac{\gamma\Theta^2}{9T^2} - \frac{1}{3} \pm 1 \quad (T \geq \Theta). \qquad \text{(I-23)}$$

The dependence of γ is again dominant. This expression has been tabulated in Table I-II and compared with the experimental data for several metals. The only conclusion to be drawn from such qualitative studies is that metals not obeying Eq. (I-23) are certainly not free-electron like. It is interesting to note that in contrast, lithium gives a reasonably good

Table I-II. Comparison of Eq. (I-23) with experimental values of (dlnR/dlnV). (Ref. 23)

Metal	Eq. (I-23)	$\left(\frac{d\ln R}{d\ln V}\right)_{observed}$
Li	2.3 ± 1	-9.9
Na	2.2	3.2
K	2.4	4.8
Rb	2.7	3.4
Cs	2.4	1.6
Al	4.4	3.1
Fe	3.3	4.0
Co	3.7	1.7
Ni	3.8	3.5
Pd	4.3	4.0
Pt	4.9	5.1
Mo	3.1	3.5
Ta	3.3	3.3
W	3.1	4.0
Pb	4.9	5.6
Cu	3.8	2.6
Ag	4.6	3.6
Au	5.9	5.1

Debye temperature from resistance data, but the comparison of Eq. (I-23) with the experimental data does not even agree in sign. Similar difficulties arise with other metals.

The effects of pressure on the residual resistance has been discussed by Dugdale and Gugan.[25] In general the sign and magnitude of the effect again depends on the type of impurity atom. The effects are usually small, but very few experiments have been performed.

Because of the complexity of the resistance process, resistivity measurements as a function of pressure cannot be used in themselves as a quantitative probe of the microscopic properties of metals. They must be complemented by other measurements such as the thermopower, Hall coefficient, magneto-resistance, and de Haas van Alphen effect. Unfortunately, these measurements are extremely difficult to perform under pressure. For a more complete analysis of the effect of pressure on the electrical resistance, see Lawson's[22] review article. Another review article by Paul[26] examines pressure effects on the electrical properties of metals in general.

The preceding sections have presented a technique for determining an equation of state in the Debye approximation. Debye temperatures may be determined from resistance-temperature data by application of the Bloch-Grüneisen equation. This data need only be combined with a single pressure-volume isotherm to completely specify the equation of state. Bridgman has supplied pressure-volume isotherms for most metals. Application of the Bloch-Grüneisen equation to aluminum at 1 atmosphere results in a Debye temperature of 395°,[14] while other values range from 385° to 411° as determined by specific heat and elastic constant data.[19] If it is assumed that aluminum continues to behave as a one electron metal

upon application of pressure this technique may be applied to obtain Debye temperatures as a function of pressure. These assumptions have been made for aluminum in applying this method to 135 kbars, which results in about a 12% decrease in volume.

C. Experimental

High pressures are obtained in this laboratory by the application of the force of a large hydraulic press to a set of opposed anvils. The opposed anvil system is based on Bridgman's principle of massive support,[27] whereby only a small portion of the anvil is used for bearing the total load of the press. The additional bulk outside the anvil faces support the load bearing face and prevent breakage. In addition, the load bearing portion of the anvil consists of cemented tungsten carbide inserted into the anvil jacket under high pressure. A typical set of Bridgman anvils is illustrated in Fig. (I-2). The dimensions of the anvil set may be altered according to the particular requirements of the experiment being performed. One-half inch anvils were used throughout this investigation.

Sample wires were made from 3 mil aluminum foil cut into 0.2 in. diameter circular hoops and annealed at 200°C for several hours. The aluminum foil was obtained from American Lamotite Corporation and found to be 99.95% pure by spectrographic analysis.

In order to provide a nearly hydrostatic medium for the transmission of the anvil pressure to the sample, the wire hoop is embedded between two silver chloride discs. Silver chloride has been found to transmit pressure nearly hydrostatically.[28] Since there are small radial pressure gradients present in silver chloride, circular sample hoops concentric with the anvil center are used to minimize this effect on the sample.

The wire-silver chloride sandwich is retained between the anvils by a pyrophyllite ($Al_2Si_4O_{12}H_2$) gasket. The gasket is coated with finely divided iron-oxide (Fe_2O_3) which increases the friction between the anvil and gasket helping to prevent a sideways extrusion of the

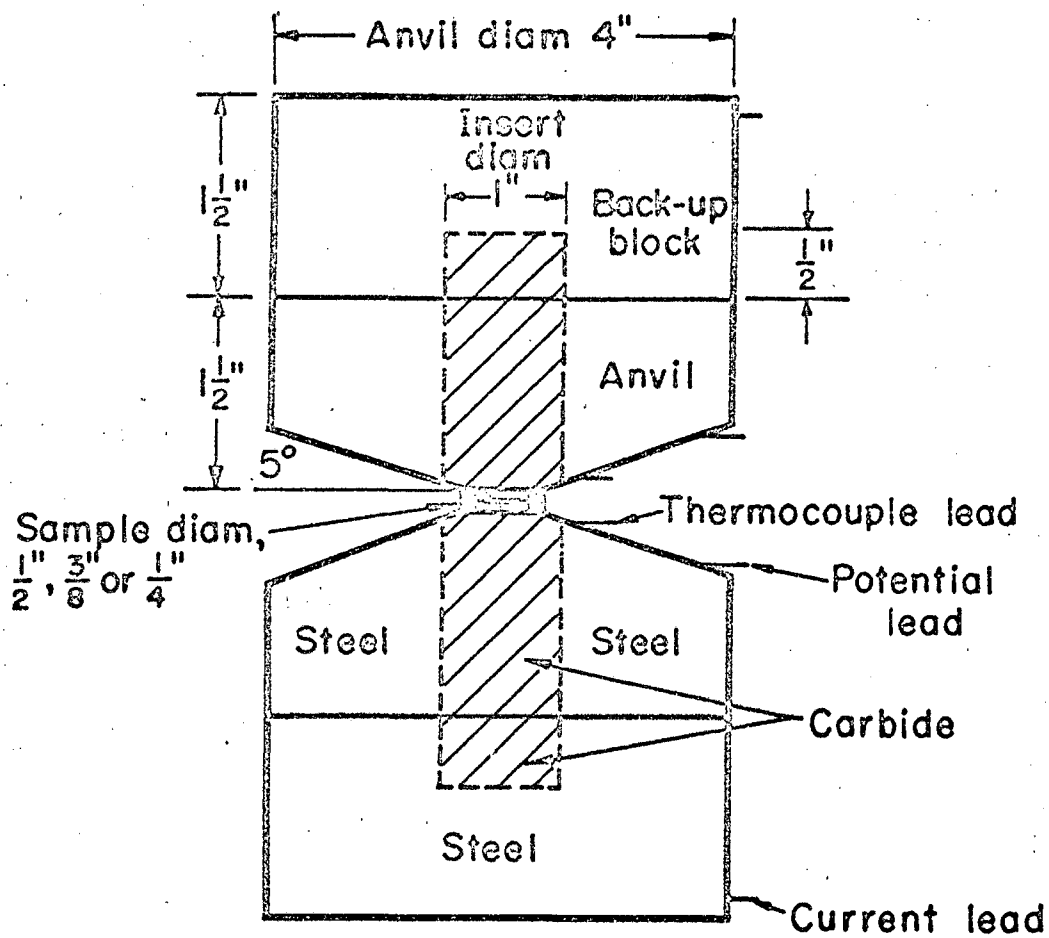

Fig. I-2 A schematic diagram of Bridgman anvils. The schematic illustrates the placement of electrical leads for making resistance measurements.

sample.

For resistance measurements contact between the anvils and sample is obtained through gold plugs inserted into small holes drilled in the silver chloride discs. Ordinarily the resistance is determined by applying a constant current across the anvils and measuring the corresponding potential drop. But the resistance determined in this manner contains contributions from contact resistances present between anvils and gold plugs and gold plugs and sample wire. These contact resistances amount to approximately 0.1 milliohms. Since the resistance of an aluminum sample of the dimensions described above is approximately 2 milliohms at 77°K, the contact resistances must be eliminated. Thus, a four-lead technique described by Stromberg and Jura[29] was applied. Potential leads consisting of 5 mil molybdenum wires are inserted directly into the pressure cell making direct contact with the sample wire and thus excluding the contact potential from the measurement. A typical sample arrangement is illustrated in Fig. (I-3). The dimensions indicated are those used throughout the investigation.

Resistance measurements are performed by applying a constant current across the anvils and observing the potential drop across the sample wire. The constant current power supply yields constant current between 5×10^{-4} and 3 amperes. The voltage was measured with a Model 149 Keithley milli-microvoltmeter in conjunction with a Speedomax two-pen recorder.

Since it was desirable to obtain resistance data to the lowest possible temperatures, a technique for pumping on a liquid nitrogen bath was developed. This extended the lowest temperatures obtainable with the high pressure apparatus from 77°K to 65°K. Because of the large mass of metal (~150 pounds) that must be cooled, 50-75 liters of liquid

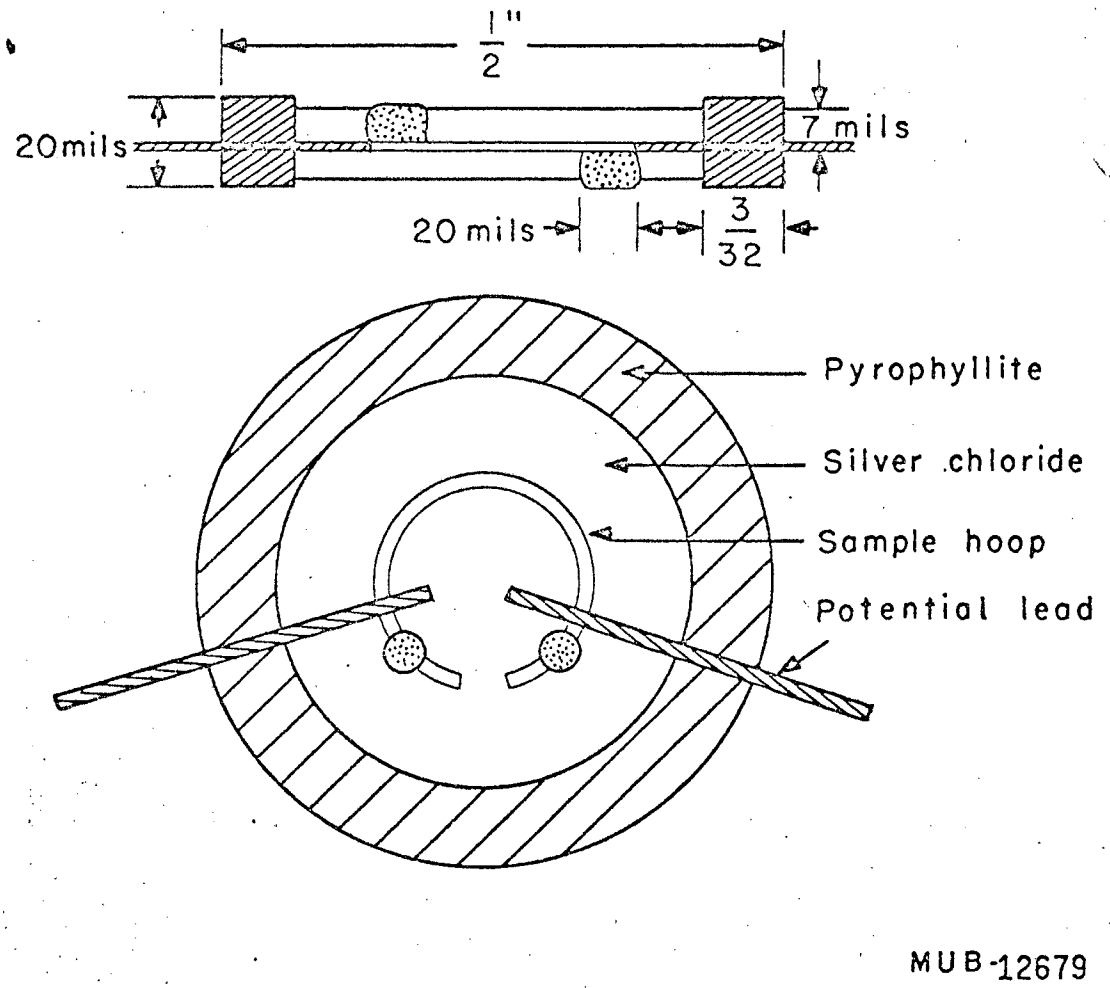

Fig. I-3 Schematic diagram of electrical resistance sample.

nitrogen and a very high pumping rate is required to reach 65°K. In order to maintain the very slow warming rate required for precise equilibrium resistance measurements, heavy copper blocks fit snuggly around the anvils and back up blocks. In addition to preventing a rapid warm-up, the copper blocks keep the top and bottom anvils at nearly the same temperature. Without the blocks, a 20° temperature gradient develops between the top and bottom anvil as the liquid nitrogen evaporates. With the copper blocks the temperature gradient may be kept at a maximum of 2° and usually less. The temperature was measured with copper-constantan thermocouples welded to the anvils as near to the sample as possible. The temperature of the sample was taken as the average of the top and bottom anvil. The thermocouples were calibrated at 77.4°K and 194.7°K with respect to a junction at 0°C. In order to account for small thermal emfs that develop across the sample, the voltage across the sample is taken as the mean value as measured with the current in opposite directions.

The average pressure on the anvil face is measured with a load cell consisting of a wire coil whose resistance changes with pressure in a known manner. The coil resistance is measured with a Baldwin-Lima SR4 bridge resulting in a measurement of the average anvil pressure to an accuracy of about 1% assuming the load cell has been calibrated properly. The oil pressure, as measured by a Heise gauge, is used in conjunction with the load cell but is accurate to only a few percent. In order to prevent the load cell from being cooled significantly by heat conduction to the cooled anvils, several bakelite blocks separate the load cell from the cooled anvils, thus maintaining the load cell temperature nearly constant.

The actual pressure of the sample wire is known from calibrations of the sample geometry in use. These are obtained by observing discontinuities

in the resistance-pressure behavior of bismuth, in which two phase transitions have been well established. These are the I-II transition at 25.5 kbars and the VI-VIII transition at 88 kbars. Based on these fixed points Montgomery et al.[28] have established a pressure scale to 125 kbars in a geometry quite similar to that used in this work. The experimental error in the pressures reported here is not known, but it is expected that the pressure scale is accurate to about 5% up to 100 kbars.

With the above techniques, resistance-temperature data were obtained from 65°K to 300°K, isobarically from 25 to 135 kbars. Several resistance-temperature isobars are shown in Fig. I-4 and similarly resistance-pressure isotherms given in Fig. I-5.

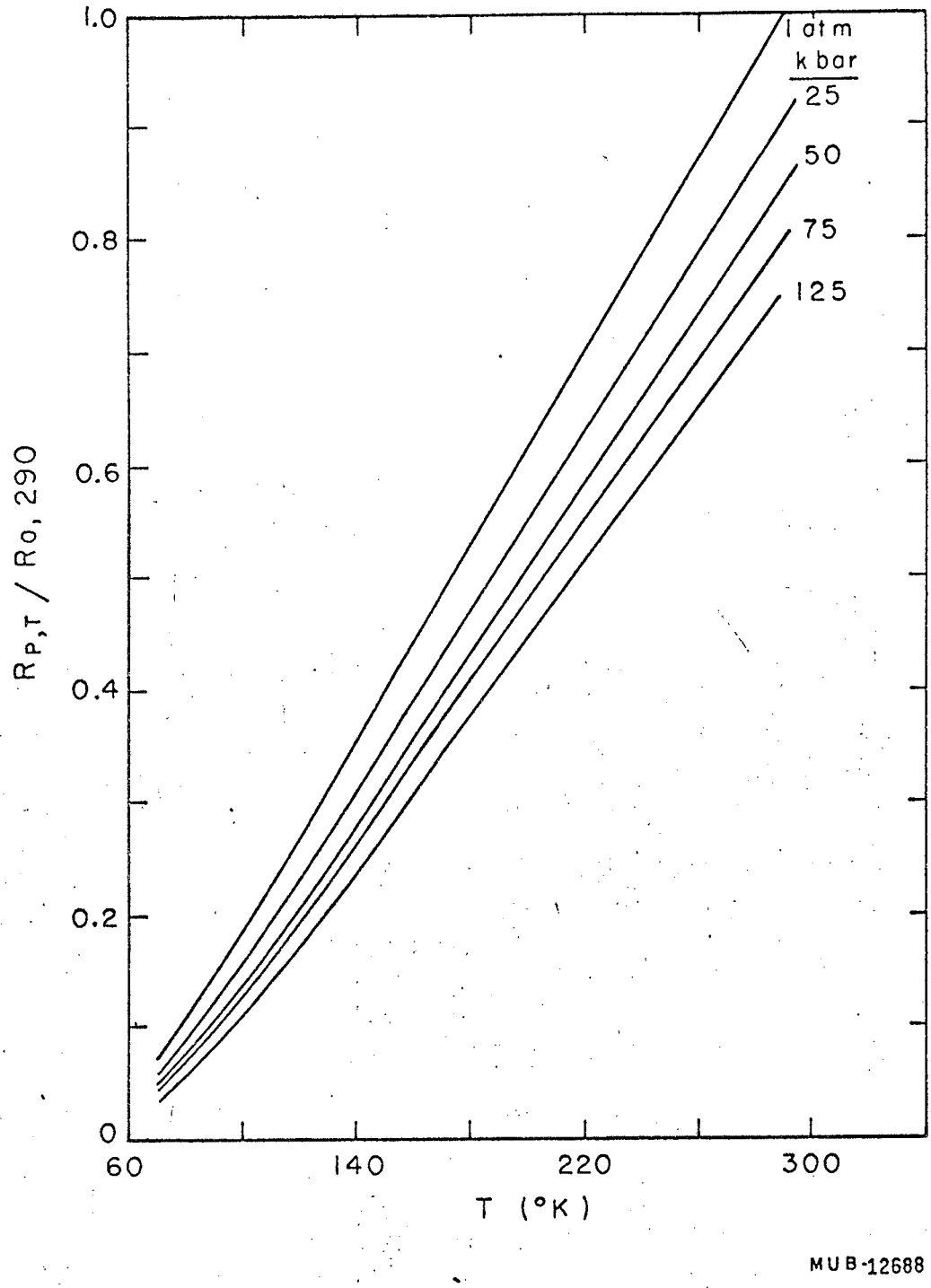

Fig. I-4 Resistance-temperature isobars for aluminum.

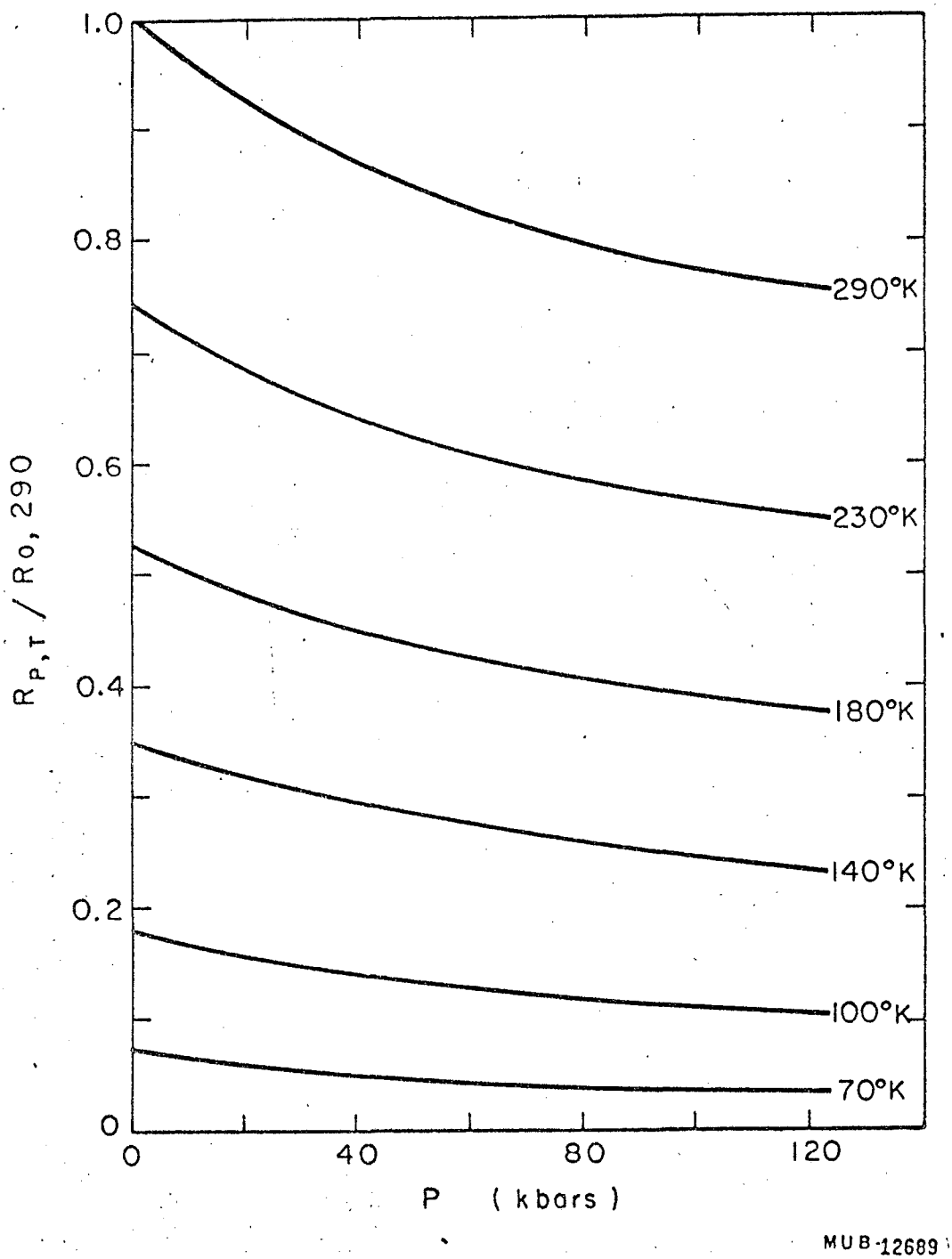

Fig. I-5 Resistance-pressure isotherms for aluminum.

D. Results

The procedure followed for the determination of the Debye temperature for each isobar will be described. First, there are two possible sources of error which affect the selection of the Debye Θ.

The first error concerns the magnitude of the residual resistivity, ρ_R, and its variation with pressure. Since the residual resistance may be measured only at low temperatures (4°K), it is impossible to find its pressure dependence in this work. The magnitude of ρ_R at 1 atmosphere was estimated from known values of similarly pure aluminum samples.[30] Typical values of $\rho_{4^\circ}/\rho_{300^\circ}$ range from 0.001 to 0.002. Assuming the pressure dependence to be small for these samples, in accordance with the results of Dugdale and Gugan,[25] application of the correction to the observed resistances raises the Debye Θ which best fits the data by about one or two degrees.

Secondly, it must be pointed out that ρ (or R) defined according to Eq. (I-19) must be observed at constant volume. All data collected in this work was obtained at constant pressure. An approximate expression which relates the constant volume resistance (R_v) to the constant pressure resistance (R_p) is given by,

$$\left(\frac{\partial R}{\partial T}\right)_V = \left(\frac{\partial R}{\partial T}\right)_P - 2\gamma\,\alpha\,R \qquad \text{(I-24)}$$

where γ is the Grüneisen ratio, and α is the thermal expansion, $\frac{1}{V}(\partial V/\partial T)_P$. Application of this correction lowers the Debye temperature which best fits the data by about two degrees. A knowledge of the pressure dependence of γ and α requires a prior knowledge of the equation of state, which is indeed unknown. Since the error in discarding this term is small, and since the correction may be applied accurately only if the equation of

state is already known, the constant pressure data is fit directly to Eq. (I-19). It is interesting to note that the two errors discussed have about the same magnitude and tend to compensate each other. Thus, unless the residual resistance increases sharply with pressure, these corrections have a negligible effect on the results.

Using the Bloch-Grüneisen equation, it would be desirable to calculate the Debye temperature from the asymtotic relationships obtained in the limit of high and low temperatures. Because of the limitations imposed on the lowest temperatures attainable with the present high pressure apparatus, it is not possible to reach sufficiently low temperatures to observe the fifth power dependence of the resistance. Because of this difficulty the experimental resistance data must be fit to the Bloch-Grüneisen equation.

Equation (I-19) has been tabulated at increments of 0.001 in Θ/T from 0 to 10 by numerical integration on an IBM 7094 computer. From these results a table was constructed of $G(\Theta/T)$ (value of Eq. (I-19) at Θ/T) versus T and Θ. The technique for choosing the best Θ for a particular isobar is simple. First, several Θ's are chosen at 5° intervals about an estimated Θ for the case. Then reduced resistance curves derived from the tables described above are calculated choosing both a high and a low temperature fixed point. The resulting tabulations are then compared with the experimental resistance data and by a suitable minimization procedure the best Θ chosen. Usually the high and low temperature fixed points gave values for Θ separated by a few degrees from which an average is taken. Figure I-6 illustrates a typical fit of the experimental data using a low temperature fixed point. The plotted data are the deviations from a curve assuming a Debye Θ of 435°. The resulting P-Θ curve is shown in Fig. I-7.

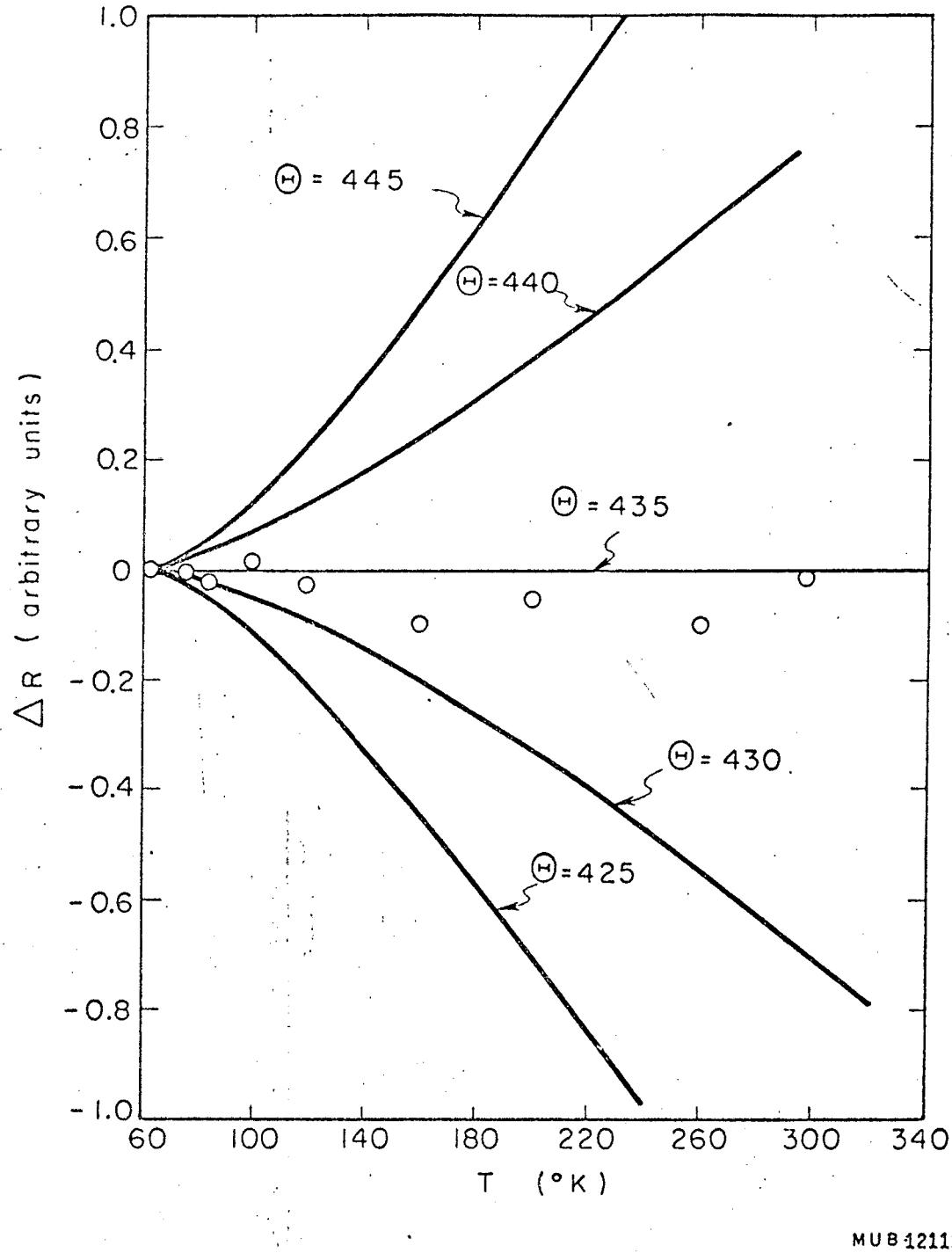

Fig. I-6 A typical fit of the experimental data using a low temperature fixed point. The deviations from an ideal resistance curve derived from Eq. (I-19) (Θ = 435°) are plotted against temperature.

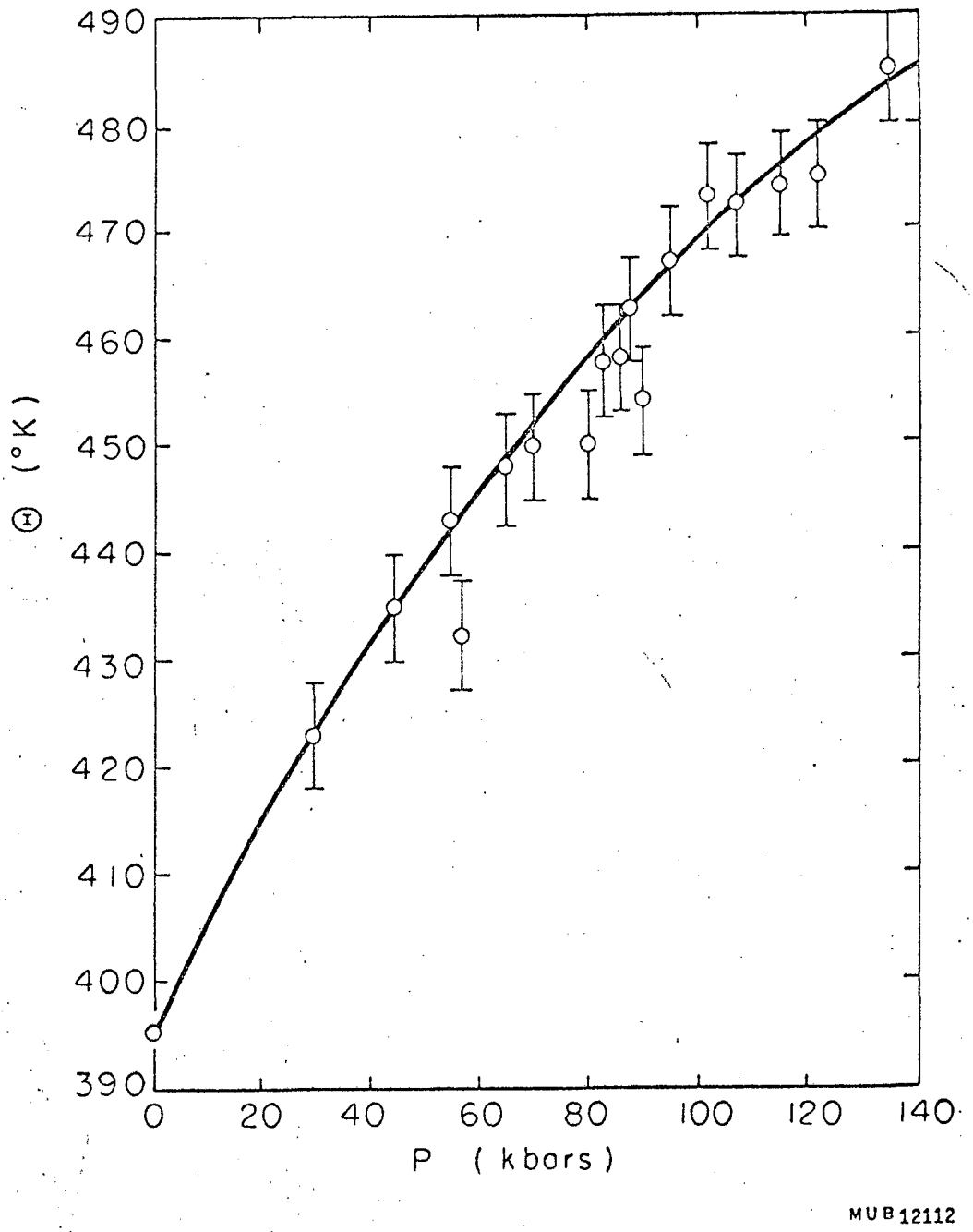

Fig. I-7 Debye temperature, Θ, versus pressure for aluminum.

The zero pressure value of 395° for Θ was obtained from previous resistance measurements.[14] The flags indicate an estimate of ±5° in the accuracy of the fit considering the experimental errors.

The required pressure-volume isotherm was obtained from a combination of results obtained by Bridgman,[31] Jamieson,[32] and Walsh and Christian.[33] This was necessary because of discrepancies in Bridgman's 100 kbar data. Since the pressure-volume data extends only to 100 kbars the equation of state is valid only to this pressure. However, the Debye temperature determinations were made to 135 kbars.

From the P-V isotherm at 298°K and the P-Θ curve obtained in this work, the variation of Θ with volume, or the more useful quantity, γ, the Grüneisen ratio, may be determined. Since the quantity γ/V or $d\ln\Theta/dV$ appears in the equation of state, $\gamma/(V/V_o)$ is illustrated in Fig. I-8. The equation of state is then obtained by tabulating the pressure variation of the vibrational energy, $(E-E_o)$ calculated from the Debye function

$$(E-E_o) = 9RT\left(\frac{T}{\Theta}\right)^3 \int_0^{\Theta/T} \frac{x^3 dx}{(e^x-1)} \quad . \qquad \text{(I-25)}$$

The variation of dE_o/dV is then calculated to complete the determination of the equation of state. The equation of state is given in tabular form in Table (I-IIIa). In addition, the pressure is tabulated as a function of temperature and reduced volume in Table (I-IIIb). dE_o/dV was integrated to obtain the total energy at absolute zero. Using the known value for the heat of vaporization at 0°K (cohesive energy) the potential curve of aluminum is illustrated in Fig. I-9, where volume has been converted to interatomic distance in the solid. The calculated interatomic distance at 0°K is 2.850Å.

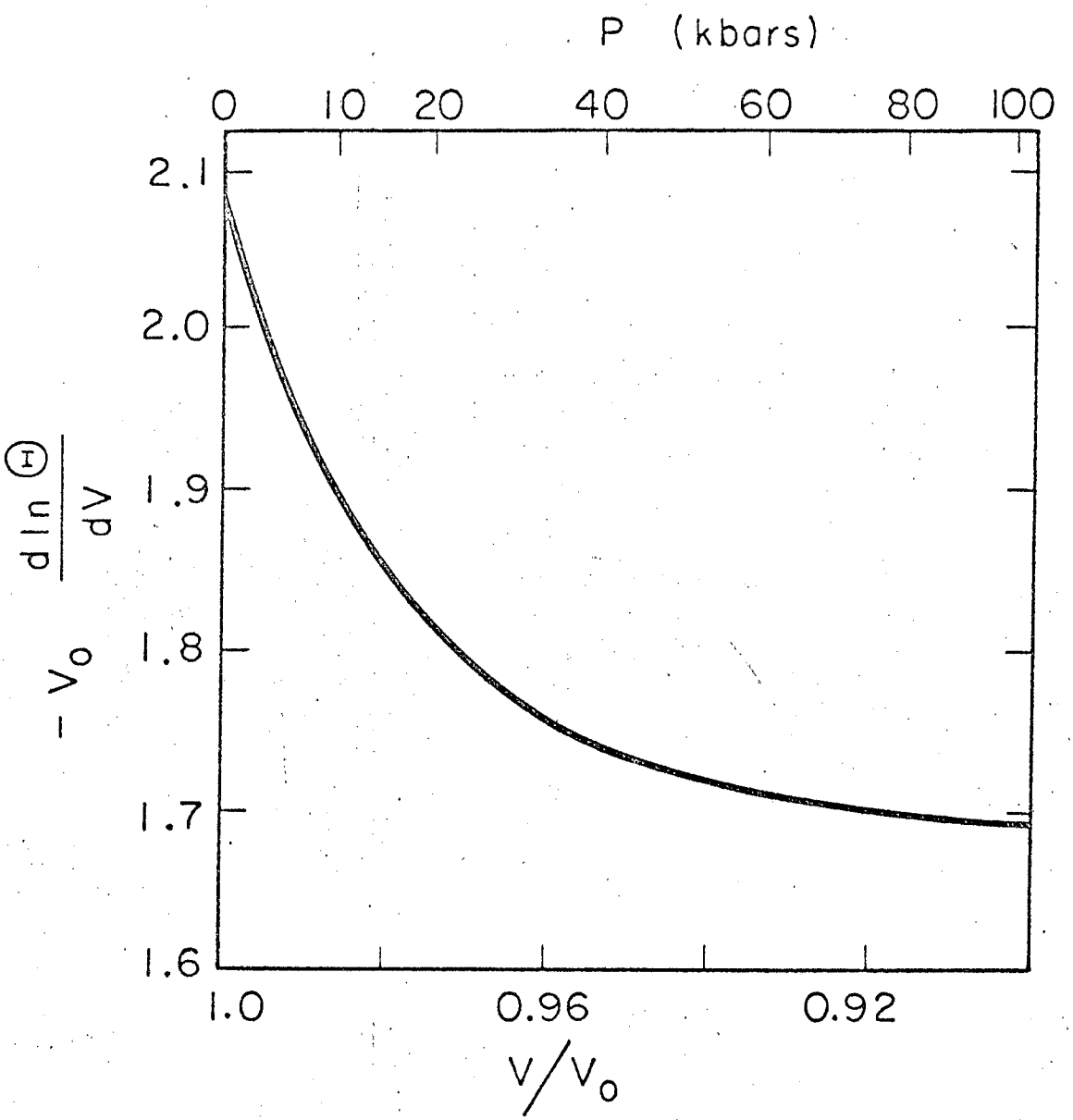

MUB-12109

Fig. I-8 Grüneisen ratio divided by reduced volume versus pressure and reduced volume.

Table I-IIIa., Equation of State of Aluminum in Tabular Form

P(kbars)	V(cc/mole) 298°K	$\frac{d\ln\Theta}{dV}$	$(E-E_o)\frac{d\ln\Theta}{dV}$ (kbars)	$\frac{dE_o}{dV}$ (kbars)
0	9.981	-.2083	-9.1149	9.1149
5	9.911	-.1978	-8.5901	3.5901
6	9.891	-.1951	-8.4621	2.4621
7.7	9.871	-.1929	-8.3422	0.6422
8.5	9.861	-.1918	-8.2544	-0.2456
10	9.841	-.1895	-8.1676	-1.8324
20	9.721	-.1805	-7.6785	-12.3215
30	9.622	-.1764	-7.4189	-22.5811
40	9.572	-.1740	-7.2377	-32.7623
60	9.312	-.1713	-6.9728	-53.0272
80	9.143	-.1699	-6.7904	-73.2096
100	9.003	-.1685	-6.6290	-93.3710

Table I-IIIb. $P = P(V/V_o, T)$ kbars

(V/V_o) \ T	298	250	200	150	100
1.000	0.00	-1.99	-3.97	-5.77	-7.22
.993	5.00	3.03	1.07	- .71	-2.14
.986	10.00	8.04	6.10	4.05	2.95
.974	20.00	18.08	16.18	14.47	13.11
.953	40.00	38.14	36.30	34.66	33.38
.933	60.00	58.18	56.40	54.83	53.62
.916	80.00	78.25	76.52	74.99	73.83
.902	100.00	98.26	96.58	95.10	93.99

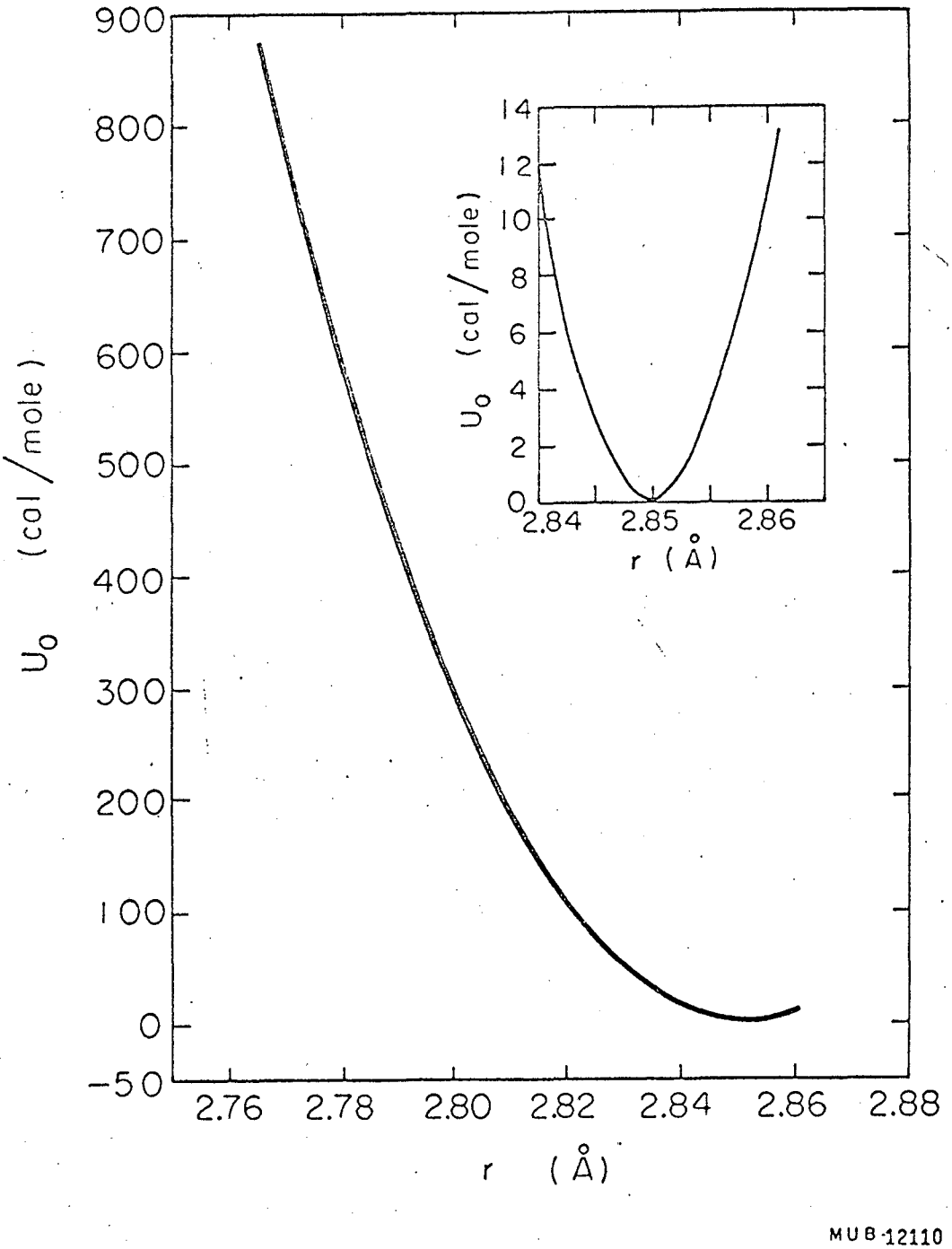

Fig. I-9 Total energy at 0°K versus interatomic distance.

Other thermodynamic quantities have been calculated using the usual thermodynamic identities. Thus, compressibility, thermal expansion, and heat capacity term (C_p - C_v) are tabulated as a function of temperature and pressure in Tables I-IV, I-V, and I-VI, respectively. Table I-VII lists the variation of E, H, A, F, and S (notation of Lewis and Randall)[36] with pressure at 298°K.

Lastly the variation of Poisson's ratio, σ with pressure and volume was calculated and is illustrated in Fig. I-10.

Table I-IV. $\left(-(\partial V/\partial P)_T \times 10^3 \text{ cc/kbar}\right)$

P \ T	298	250	200	150	100
0	13.48	13.26	13.04	12.85	12.66
10	12.62	12.42	12.21	12.02	11.87
20	11.80	11.62	11.42	11.25	11.12
40	10.29	10.14	9.98	9.82	9.71
60	8.95	8.72	8.64	8.55	8.48
80	7.78	7.67	7.56	7.47	7.39
100	6.76	6.68	6.60	6.54	6.48

Table I-V. $\left((\partial V/\partial T)_P \times 10^5 \text{ cc/deg}\right)$

P \ T	298	250	200	150	100
0[34]	69	65	60	50	34
0	64.1	61.0	55.9	48.8	34.4
10	54.5	53.2	49.2	42.8	29.7
20	48.7	47.0	43.6	37.7	25.8
40	40.1	38.1	35.5	30.4	20.2
60	34.0	32.3	29.9	25.1	16.5
80	29.2	28.1	25.8	21.5	13.9
100	24.3	23.5	21.3	17.6	11.3

Table I-VI. $(C_p - C_v)$ cal/deg mole.

P \ T	298	250	200	150	100
0^{35}	.220	.166	.112	.064	.022
0	.224	.172	.117	.068	.023
10	.171	.138	.096	.055	.018
20	.144	.114	.080	.045	.014
40	.110	.085	.060	.033	.010
60	.091	.070	.049	.027	.008
80	.079	.062	.042	.023	.006
100	.066	.053	.035	.018	.005

Table I-VII. Thermodynamic Functions, 298°K cal/mole

P	ΔU	ΔH	ΔA	ΔF	ΔS*
0	0	0	0	0	0
10	-28	2324	14	2366	-0.10
20	-21	4634	58	4714	-0.24
40	74	9174	213	9314	-0.46
60	256	13616	451	13810	-0.64
80	493	17983	734	18221	-0.80
100	748	22268	1025	22545	-0.92

* cal/deg mole

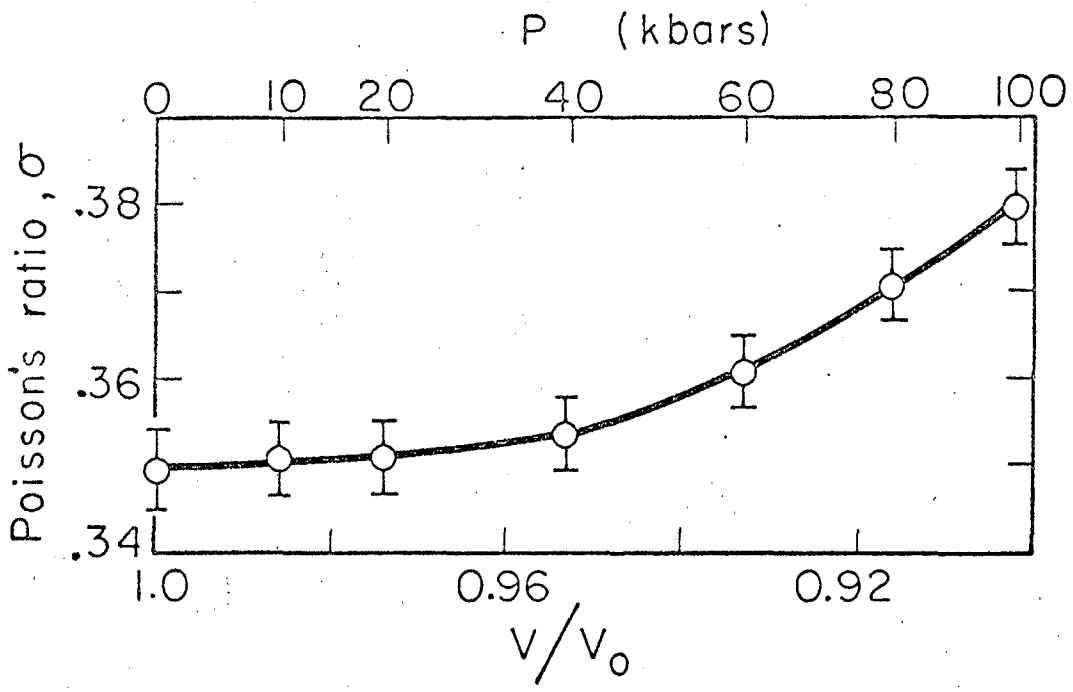

MUB-12113

Fig. I-10 Poisson's ratio versus pressure and reduced volume.

E. Discussion

When a solid is compressed the force constants between the atoms of the lattice are increased and the corresponding vibrational frequencies are also increased. Since the Debye temperature is directly proportional to the maximum lattice frequency, it is expected to increase with pressure. This effect was observed for aluminum and shown in Fig. I-7. Increasing the pressure to 135 kbars decreases the volume by about 12%, but the corresponding increase in the Debye temperature is almost 23%. The Debye Θ increases from 395° at 1 atomosphere to 485° at 135 kbars. Of course, the rate of increase of the Debye temperature with volume is given by the Grüneisen ratio, γ, defined by Eqs. (I-9) and (I-11). Differentiation of the observed Θ-V curve yields a zero pressure value of γ equal to 2.08. This value is in good agreement with the value 2.19±0.10 obtained from thermodynamic data.[19] Also, since all the data collected here was obtained above 25 kbars, the calculated value of γ indicates that the fit in the region between 0 and 25 kbars is valid. The Grüneisen ratio is found to decrease with volume.

Figure (I-8) illustrates the behavior of $\gamma/(V/V_o)$ which decreases gradually to about 40 kbars whereupon it levels off to a constant value of approximately 1.70. Kormer et al.[37] have determined the Grüneisen ratio for aluminum in shock wave experiments from 700 kbars to several megabars. They have extrapolated their data to zero pressure using a value of 2.13 for γ obtained from 1 atmosphere thermodynamic data. Kormer finds that $\gamma/(V/V_o)$ is approximately constant up to 600 kbars and equal to 2.08. Although a direct comparison cannot be made between this work and that of Kormer, it is worthwhile pointing out that his data does indicate that γ/V is approximately constant in the region of pressures applicable in this work.

The value of $\gamma/(V/V_o)$ which best fits the data obtained from 0 to 100 kbars is 1.78. The equation of state is then approximated by the analytical expression

$$\Theta = 395\, e^{-1.78\, \Delta V/V_o} \qquad \text{(I-26)}$$

The exponential dependence of the frequency on volume leads one to believe that a Morse potential might describe the total energy of the system. The bonds between atoms in a metal are certainly not entirely different in their properties from the bonds of homopolar molecules. The internal energy of the system is given by the Morse function

$$E_o = L(e^{-2A(r-r_o)} - 2e^{-A(r-r_o)}).^{38} \qquad \text{(I-27)}$$

E_o represents total crystal energy at absolute zero as a function of nearest neighbor distance, r, where r_o represents the equilibrium value of r and L is the heat of vaporization or the cohesive energy at 0°K. The quantity A is an empirical constant. The Morse curve which best fits the potential curve calculated above and illustrated in Fig. I-9 is

$$E_o = 76.9\, (e^{-2 \cdot 1.20(r-2.850)} - 2e^{-1.20(r-2.850)}). \qquad \text{(I-28)}$$

L is given in kcal/mole and r in angstroms. Pastine[39] has applied similar arguments to several face-centered cubic metals including aluminum but his work is directed primarily to comparisons with shock-wave data. As does Kormer, Pastine uses the thermodynamic value of γ at zero pressure. The calculated behavior of γ/V is analogous to that of Kormer, $\gamma/(V/V_o)$ is approximately constant and equal to 2.17 up to approximately 500 kbars. The empirical constant A used by Pastine in Eq. (I-27) is 1.33 compared with 1.20 found here. Also, he calculated a change in the Debye temperature

of 85 degrees for a pressure of 100 kbars compared with 75 degrees found in this work.

Returning to the internal energy illustrated in Fig. I-9, the calculated minimum at 2.850Å compares quite favorably with the value of 2.851Å found from extrapolation of x-ray data to 0°K.[40] It is pointed out that the region of energy studied in this investigation (~1 kcal) represents a very small percentage of the total energy of the crystal (76.9 kcal/mole).

The isothermal compressibility coefficient $(\partial V/\partial P)_T$ tabulated in Table I-IV needs little discussion. The small temperature dependence is expected, since the compressibility is primarily a function of the total energy at absolute zero, which changes very slowly with pressure as discussed above.

The coefficient of thermal expansion $(\partial V/\partial T)_P$ tabulated in Table I-V shows a marked pressure dependence. This again is not surprising because of the large energies associated with pressure-volume changes compared with thermal energies. A similar behavior is observed for the heat capacity term $(C_P - C_V)$ tabulated in Table I-VI. Tables I-V and I-VI include comparisons with zero pressure thermodynamic data. The agreement is within a few percent overall. The heat capacities C_P and C_V are easily obtained from the Debye temperatures reported in conjunction with Table I-VI.

Figure I-11 illustrates the comparison between the heat capacity, C_P, determined here at 50 kbars and that of Stark determined by direct measurement of C_P of aluminum at 50 kbars. The agreement is excellent and increases my confidence in this equation of state.

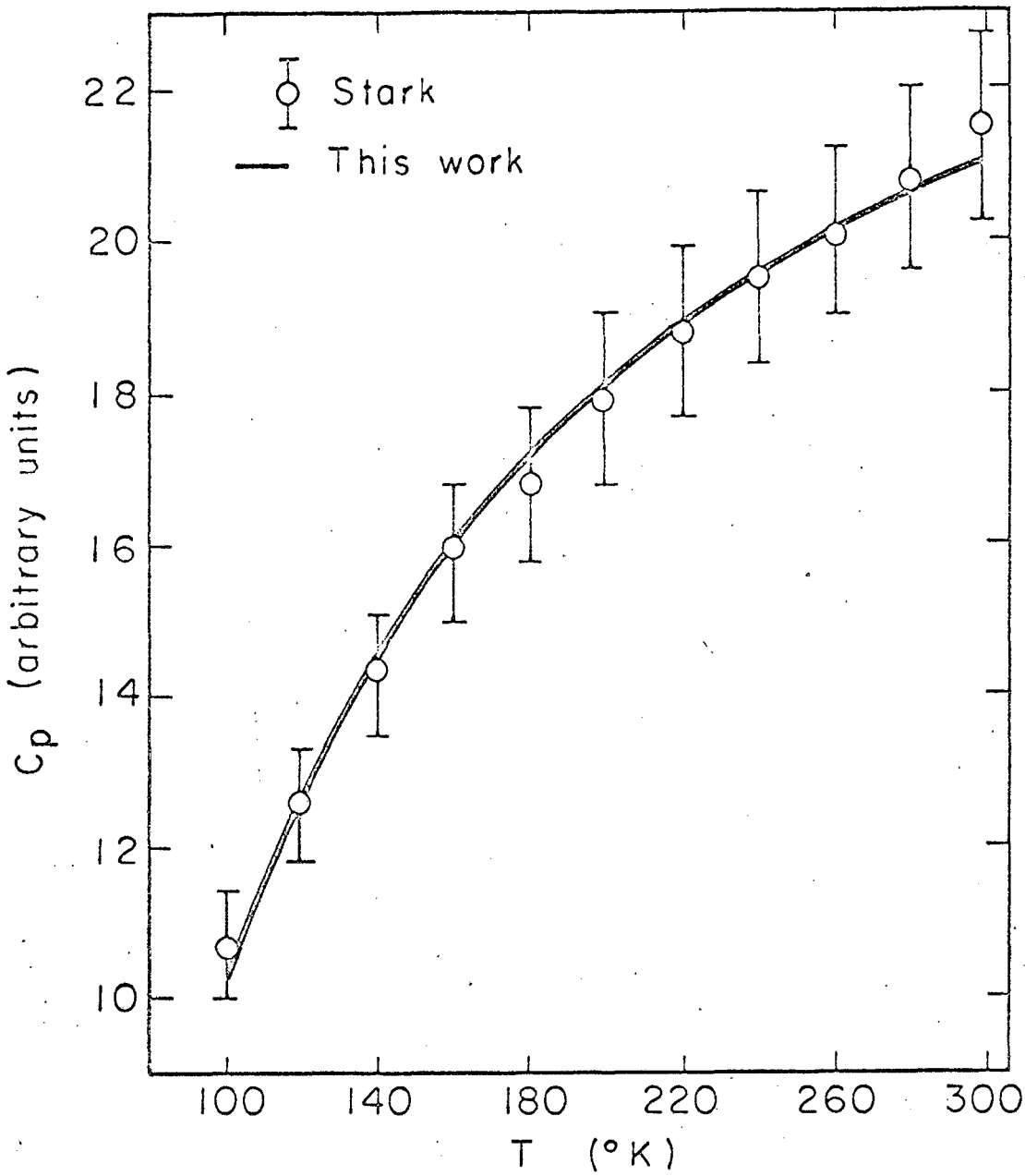

MUB-12108

Fig. I-11 Heat capacity of aluminum at 50 kbars compared with preliminary data of Stark (unpublished data).

Poisson's ratio, illustrated in Fig. I-10, is defined as the ratio of the longitudinal extension to the transverse contraction of a thin rod. The zero pressure value of σ is 0.350 and is found to be nearly independent of pressure up to about 40 kbars where it begins to increase slowly to a value of 0.38 at 100 kbars. This result is in agreement with elastic constant determinations up to 10 kbars,[41,42] where Poisson's ratio is found to be independent of pressure. Utilizing the elastic constant data further, Debye temperatures were calculated. The Debye Θ is found to have a somewhat greater volume dependence than observed here. The initial value of the Grüneisen ratio is 2.50, which is considerably larger than the thermal value 2.19 and the value 2.08 determined here. Extrapolation to 100 kbars yields a Debye temperature 13% greater than observed here.

Lastly, the thermodynamic functions tabulated in Table I-VII require little discussion. They show no irregularities which question the validity of the equation of state. Slater[43] has discussed the pressure variation of the thermodynamic functions of other simple metals. This discussion applies equally well to the results on aluminum obtained in this work.

F. Conclusions

The overall agreement of the results calculated here with other experimental data is very encouraging. The idea that aluminum behaves as a simple one electron metal over the entire pressure range investigated appears to be well founded. Of course, an exact evaluation of the procedure used in this work awaits further theoretical and experimental developments. Measurements of the heat capacity in this laboratory will certainly aid our understanding of metals under high pressure conditions and help to verify or nullify the results of this work. Considering the apparent success of this study, it would be worthwhile to extend this procedure to other simple metals, especially the alkali metals which show large volume changes and have received a great deal of attention both theoretically and experimentally. The Debye temperature of lithium should increase from 363° to over 500° at 100 kbars. But because of the unusual behavior of the resistance of lithium with pressure, the Bloch-Grüneisen theory may not apply at all under pressure.

Another interesting application of this technique would be the determination of the change in the Debye temperature across a phase boundary, thus determining the change in the entropy for the transition. A particular case where this technique is applicable is the phase transition in tin at 110 kbars.

In conclusion, the experimental technique described above has proven to be quite successful in its application to aluminum. The measurements are quite easy to perform and a minimum of instrumentation is required. Because the technique relates two seemingly unrelated topics, electrical resistance to equation of state, it is very interesting both theoretically and experimentally.

II. EFFECT OF PRESSURE ON THE MÖSSBAUER SPECTRUM OF Fe^{57} IN IRON AND NICKEL METAL

A. Introduction

The Mössbauer effect has served as an important tool in investigating the interaction of the nucleus with its environment. Although the Mössbauer effect is essentially a nuclear phenomena, the electronic environment to which the nucleus is subjected plays an important role in analysis of the results of Mössbauer experiments.

Although the variation of the interatomic distance in the solid may result in a profound change in the Mössbauer spectrum of a given system, relatively few high pressure Mössbauer studies have been reported. High pressure Mössbauer studies on Fe^{57},[44,45,46] Sn^{119},[47] and Dy^{161},[48] have only scratched the surface of experiments which are required to fully understand the relationship of the nuclear parameters to the bulk properties of solids.

In the present investigation, the Mössbauer effect of Fe^{57} in iron and nickel is studied as a function of pressure. Iron was studied up to a pressure of 140 kbars, with particular interest in the high pressure phase transition of iron to the hexagonal phase. Nickel metal was studied up to 80 kbars, with emphasis on the low pressure region. The results are discussed in terms of the relationship of the observed nuclear parameters to the bulk properties of these metals.

B. Theory

1. General

Several comprehensive reviews of the Mössbauer effect and its applications in physics and chemistry are readily available in the literature.[49,50] This discussion is thus limited to a discussion of the Fe^{57} Mössbauer effect and its pressure dependence. Fe^{57} is produced by the electron capture decay of Co^{57} which has a 270 day half-life. The decay of Co^{57} to Fe^{57} and the properties of the Fe^{57} nucleus are illustrated in Fig. II-1.

Prior to the work of Mössbauer, gamma ray emission was considered to be a free atom phenomena. Conservation of energy and momentum require the emitting nucleus recoil with an energy, E_R, given by

$$E_R = \frac{E_\gamma^2}{2Mc^2} \qquad \text{(II-1)}$$

where E_γ is the gamma ray energy, M is the nuclear mass, and c is the speed of light. The difference between the nuclear transition energy, E_o, and the gamma ray energy, E_γ, consists of the free atom recoil energy, E_R, plus a Doppler effect caused by the thermal velocity of the emitting nucleus. The fraction of the available energy lost to the recoiling atom is small; for the 14.4 keV gamma ray from the decay of Fe^{57}, the recoil energy is only 1.9×10^{-3} ev. The energy loss does become significant, however, when compared with the inherent width of the gamma ray as determined by the uncertainty principle of energy and time,

$$\tau\,\Gamma = h/2\pi \qquad \text{(II-2)}$$

where τ is the lifetime of the nuclear state, Γ is the linewidth of the gamma ray, and h is Planck's constant. The linewidth for the 14 keV

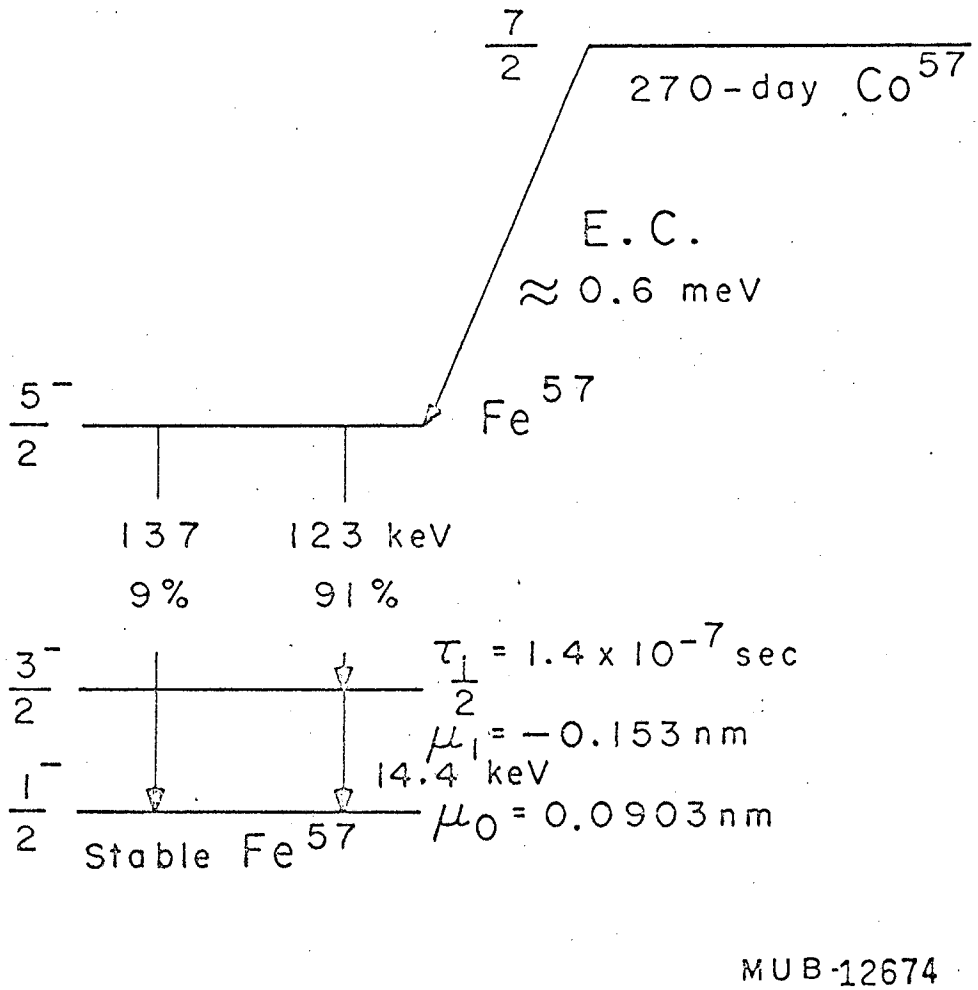

Fig. II-1 The decay of Co^{57} to Fe^{57} and the properties of the Fe^{57} nucleus (after Wertheim[50]).

state of Fe^{57} is 4.55×10^{-9} eV, which is very much smaller than the energy loss in nuclear recoil. As a result, the gamma ray emission line does not overlap the absorption line, and nuclear resonance absorption is not observable. This situation is illustrated in Fig. II-2.

Mössbauer[51] found that when low energy γ-rays are emitted from nuclei that are embedded in a solid with a large effective Debye temperature, Θ_D, there exists the possibility that a sizeable number of the transitions will occur without recoil. This situation arises because the effective recoiling mass becomes the mass of the whole crystal. Thus, M in Eq. (II-1) increases by approximately 10^{23}, and as a consequence E_γ is essentially equal to the nuclear transition energy, E_o. The fraction of recoil-free events, f, is given in a Debye approximation by

$$f = \exp\left[-\frac{6E_R}{k\Theta_D}\left(\frac{1}{4} + \left(\frac{T}{\Theta_D}\right)^2 \int_0^{\Theta_D/T} \frac{x\,dx}{e^x-1}\right)\right], \qquad \text{(II-3)}$$

where T is the temperature and k is Boltzmann's constant.[50] Only those γ-ray transitions in which the entire crystal recoils, and no vibrational modes are excited, will possess essentially the full transition energy, E_o. Thus, nuclear resonance is observable if the above conditions are met by both source and absorber. The particular usefulness of the Mössbauer effect lies in the narrowness of the observable linewidths. The fractional linewidth for Fe^{57} when compared with the gamma ray energy is 3×10^{-13}. This is equivalent to the statement that the energy of the gamma ray is defined to within three parts in 10^{13}! Furthermore, the linewidth is smaller than characteristic values for the magnetic dipole and electric quadrupole interactions of nuclei with their surrounding electrons.

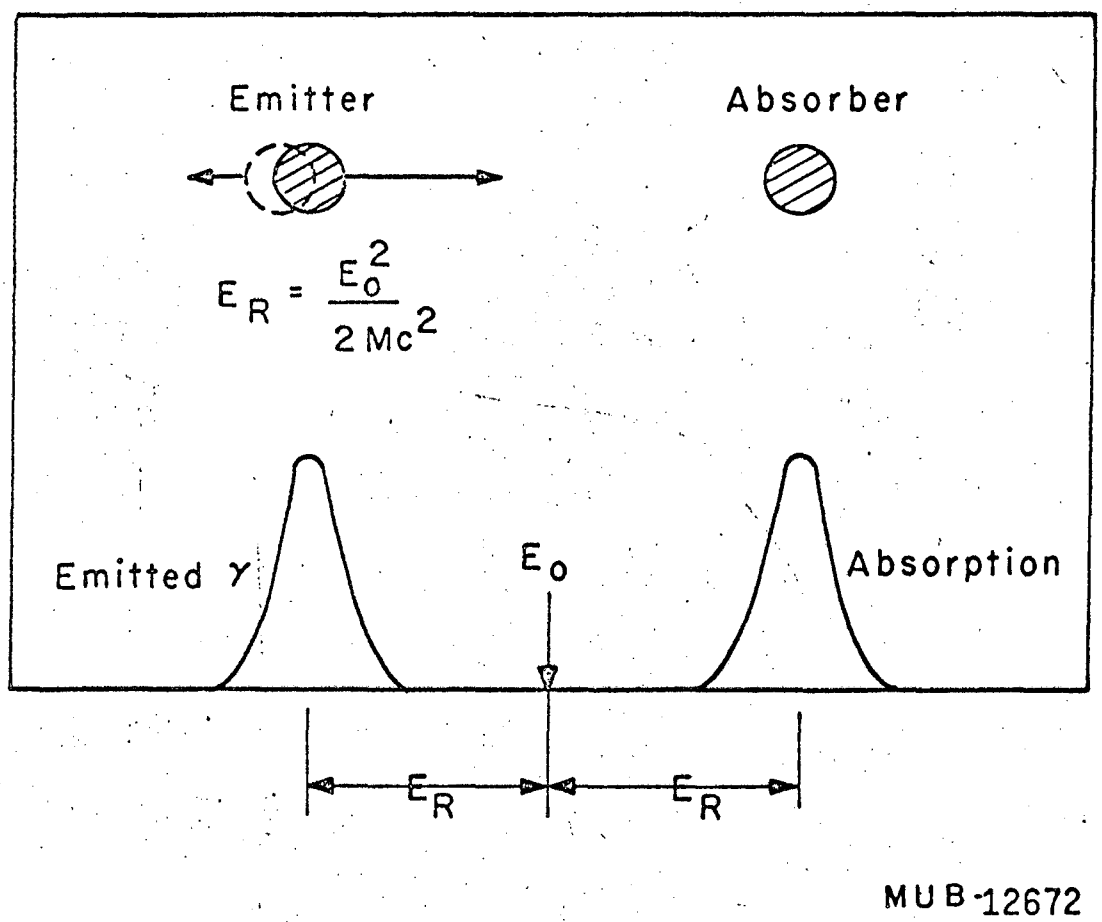

Fig. II-2 Free atom gamma ray emission and absorption lines.

The resonance condition is observed by applying a relative velocity, v, between source and absorber which varies the energy of the gamma ray by a Doppler shift, ΔE, given by

$$\Delta E = \frac{v}{c} E_{\gamma}. \qquad \text{(II-4)}$$

As the relative velocity increases, the resonance condition is destroyed. The profile of the resonance effect is given by a Lorentz curve which has the form

$$\sigma(E) = \frac{\sigma_m}{\left[\frac{2}{\Gamma_a}(E-E_o)\right]^2 + 1} \qquad \text{(II-5)}$$

where $\sigma(E)$ is the absorption cross section at energy E, Γ_a is the full width at half maximum of the absorption line, and σ_m is the maximum cross section.[52]

The Mössbauer effect is of particular interest in the physical sciences because it serves as a delicate probe of small perturbations on the energies of the nuclear levels of source and absorber. The energy levels of the source or absorber are perturbed by the interaction of the nucleus with the environment. Usually the source and absorber environment are not identical because of the possible occurrence of

i) differing Coulombic energies of source and absorber

ii) interaction of the nuclear quadrupole moment with the electric field gradient at the nucleus

iii) internal magnetic fields causing a Zeeman splitting of the nuclear levels.

The result of (i) is commonly called the isomer or chemical shift, which is the displacement of the center of gravity of the spectrum from

zero velocity. If the ground and excited state charge radii, R_{gd} and R_{ex}, are unequal, the levels experience different electrostatic interactions which result in an unequal shift of the nuclear levels. The isomer shift between the source and absorber is given by

$$\text{I.S.} = \frac{2\pi Ze^2}{5}\left(R_{ex}^2 - R_{gd}^2\right)\left[\psi(0)^2_{abs} - \psi(0)^2_{source}\right] \qquad \text{(II-6)}$$

where $\psi(0)^2_{abs}$ and $\psi(0)^2_{source}$ are the electron densities at the nucleus of absorber and source, respectively.[50] In a non-relativistic approximation, the electron density at the nucleus is appreciable only for s electrons. The first systematic interpretation of isomer shifts was made by Walker et al.[53] Figure II-3 illustrates the graph they have constructed for isomer shifts relative to stainless steel for several substances containing Fe^{57}. This illustration can be useful in estimating the electronic configuration of a material from Mössbauer data. Shirley has provided an excellent paper on the application and interpretation of isomer shifts.[54]

In addition to the isomer shift there is a second-order Doppler effect due to the thermal motion of the atoms.[55] The shift in energy for a unit temperature difference may be written

$$\frac{\partial}{\partial T}\left(\frac{\delta E}{E}\right) = -\frac{C_p}{2c^2}, \qquad \text{(II-7)}$$

where C_p is the heat capacity of the solid. This shift is, of course, not observable unless source and absorber are at different temperatures. For Fe^{57} in iron the experimental shift is $2.1\times10^{-15}/^\circ K$ at room temperature.[55] This amounts to a shift of about one linewidth for a difference of $300^\circ K$ in the temperatures of source and absorber.

An energy level with a nuclear spin moment of odd half integral I has an (2I+1)-fold degeneracy in a spherically symmetric electric field.

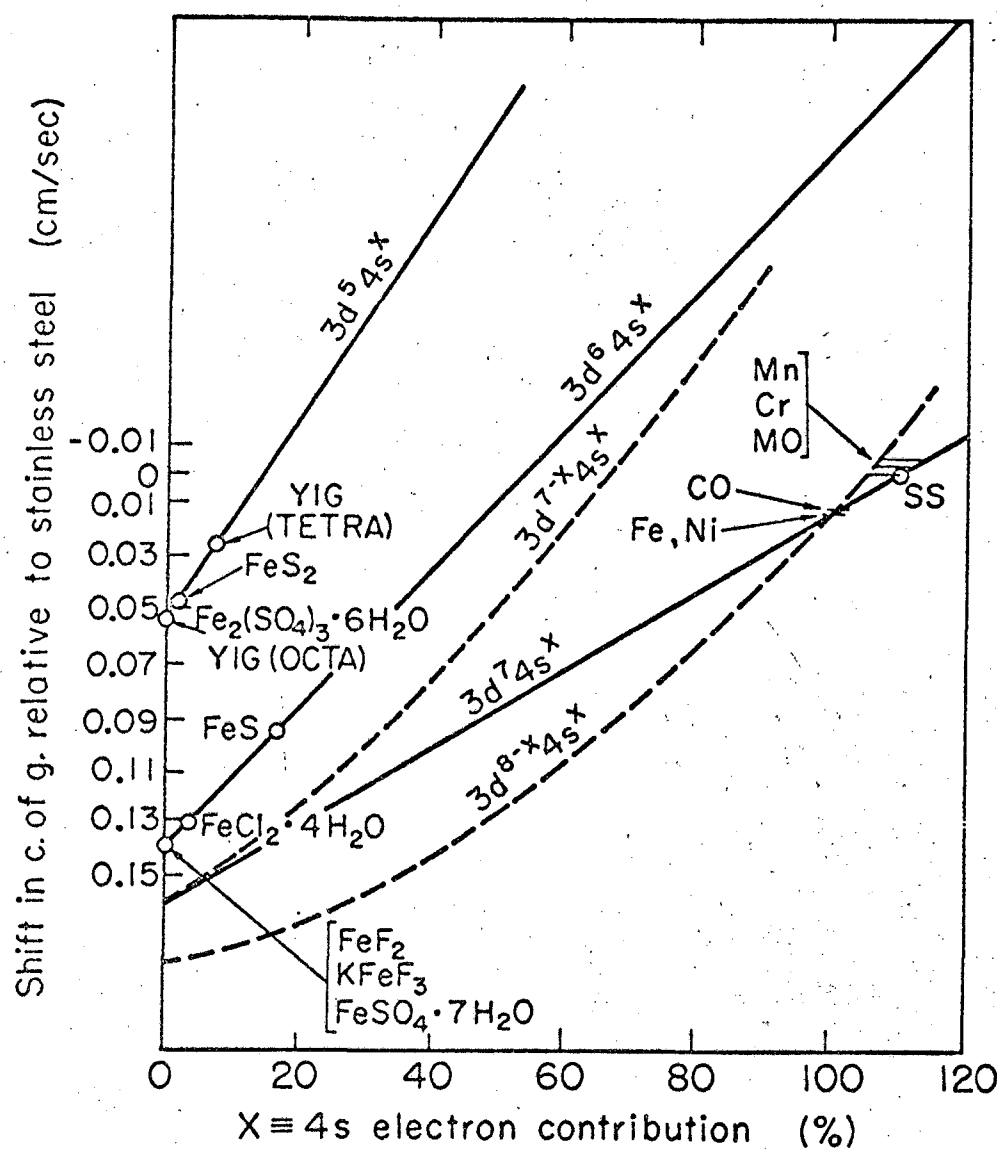

MU-31352

Fig. II-3 The dependence of the chemical shift on the electronic configuration of iron (after Walker et al.[53]).

The degeneracy is partially removed when there is an electric field gradient at the nucleus, whereby the nuclear level splits into (I+1/2) components. The field gradient, which is the second derivative of the potential with respect to the coordinate, is usually expressed in terms of $(\partial^2 V/\partial Z^2) = eq$ and the asymmetry parameter

$$\eta = \frac{\partial^2 V/\partial Y^2 - \partial^2 V/\partial X^2}{\partial^2 V/\partial Z^2} \quad . \qquad \text{(II-8)}$$

Using this notation, the interaction between the nuclear quadrupole moment, eQ, and the electric field gradient is given by

$$\Delta E_Q = \frac{e^2 qQ}{4I(2I-1)} \left(3m^2 - I(I+1)\right)\left(1 + \frac{\eta^2}{3}\right)^{1/2} \qquad \text{(II-9)}$$

where the magnetic quantum number m has values I, I-1, ..., -I.[50]

When a nuclear level has a non-zero spin, the resulting magnetic moment μ, may interact with a magnetic field, H, arising either internally or by application of an external field. Under such conditions, a nuclear Zeeman effect is observed. The nuclear level is then split into (2I+1) components given by

$$E_m - E_o = -\frac{m}{I}\,\mu H \qquad \text{(II-10)}$$

The selection rules for magnetic dipole radiation are $\Delta m = 0, \pm 1$. This produces six possible transitions for Fe^{57} for which $I_{ex} = 3/2$ and $I_{gd} = 1/2$. The relative intensities of these lines depends on the orientation of the magnetic field with respect to the emission axis, but for a polycrystalline specimen the intensities are averaged over a sphere. The resulting intensities are 3:2:1:1:2:3 (in the order of increasing energy). The emission spectrum of the 14.4 keV excited state of Fe^{57} is illustrated in Fig. II-4.

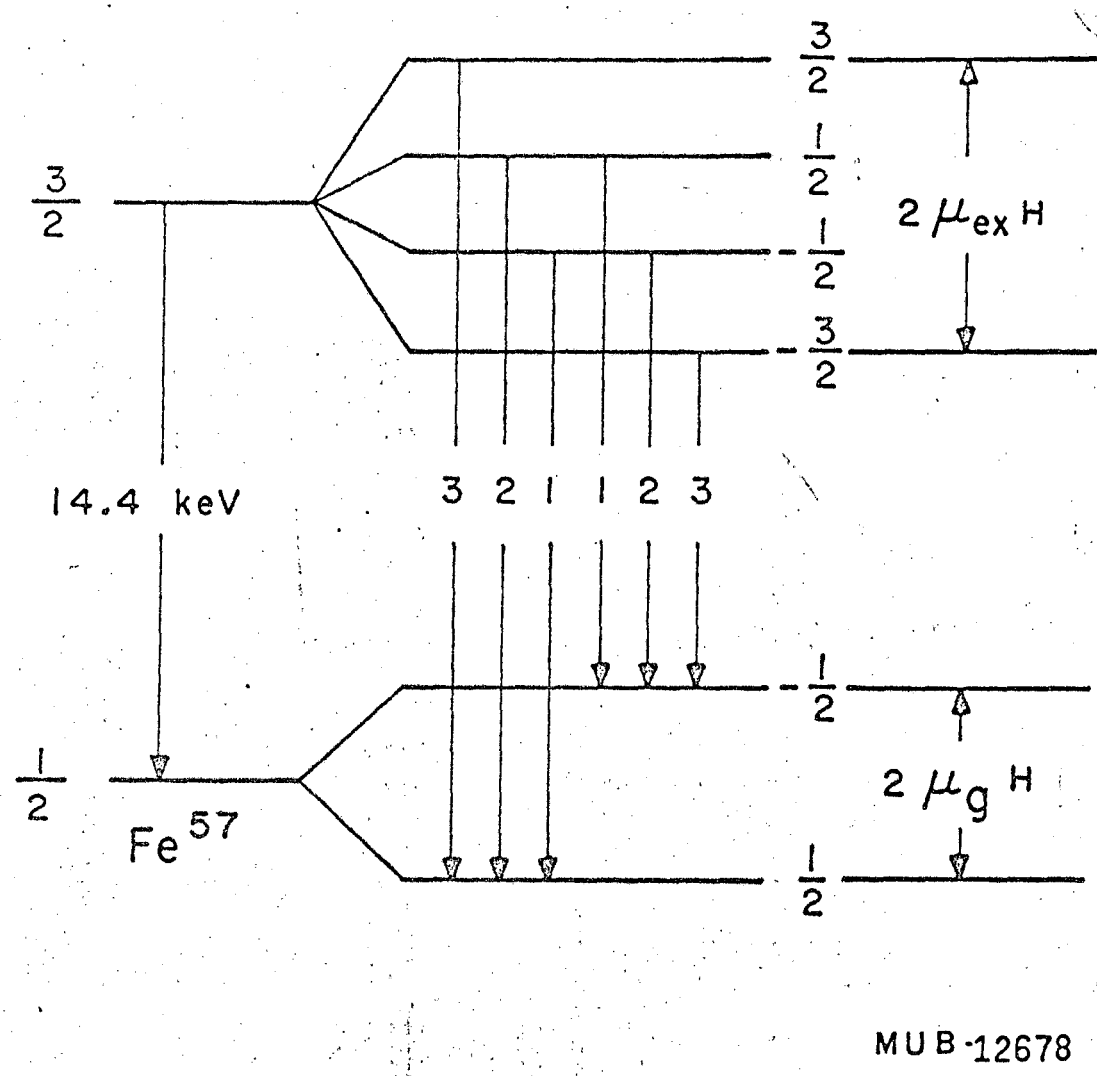

Fig. II-4 Emission spectrum of the 14.4 keV excited state of Fe^{57}.

Mössbauer studies of the Zeeman effect in iron have shown that the magnetic field at the nucleus of Fe^{57} is large (-330 kilogauss) and in the opposite direction to the magnetization.[56] The origin of the internal magnetic field has been discussed by Marshall[57] and Watson and Freeman.[58] There is a small contribution (+ 70 kg) produced by the unquenched orbital angular momentum of the 3d electrons. But the major contribution arises from the field proportional to the spin density at the nucleus as a result of the Fermi contact interaction. The spin density arises partly from the core electrons, therefore, the 1s, 2s, and 3s electrons localized on the parent atom and partly from the conduction electrons. The core contribution arises from polarization of the 1s, 2s, and 3s electrons by the spin aligned d-electrons. Watson and Freeman[58] have estimated a core contribution of -350 kg to the hyperfine field in pure iron. The spin density of the conduction electrons has been considered by Anderson[59] and Anderson and Clogstrom[60] and arises from polarization produced by exchange interactions with the 3d electrons and by admixture with the 3d band. The resultant spin density due to 4s electrons may be of either sign. Since the important contributions to the internal field are proportional to the mean spin per atom, the field is therefore proportional to the saturation magnetization, σ. This can be written

$$H = A\sigma, \qquad \text{(II-11)}$$

where A is the hyperfine coupling constant. In studies of Fe^{57} in iron from low temperatures to the Curie point,[61,62] it is found that the internal field of Fe^{57} is approximately proportional to the magnetization over the entire range. Similar findings have been obtained in nuclear magnetic resonance studies of other pure metals, such as Ni^{61} in nickel[63] and Co^{59} in cobalt.[64] Benedek[65] has shown that small deviations arise

from a slight temperature dependence of the coupling constant, A. Significant deviations from proportionality have been observed in dilute alloys, such as Fe^{57} in nickel,[66] Mn^{55} in iron,[67] and Co^{59} in nickel.[68] These deviations have been explained in terms of localized impurity moments. In other words, there are localized spin deviations at the impurity atoms which are coupled either strongly or weakly to the host magnetization.

2. Effect of Pressure on Mössbauer Effect

By measurement of the Mössbauer spectrum of a source under pressure, information about the volume dependence of the internal magnetic field and electric field gradient at the nucleus, the electron density at the nucleus through the variation of the isomer shift, and the lattice properties through the second-order Doppler shift and recoil-free fraction may be obtained. Also, discontinuities in any of these parameters may reflect the occurrence of a phase transformation.

Hanks[69] has discussed the change of the recoil-free fraction, f, with pressure. Making use of Eq. (II-3) for the value of f in the Debye approximation and the Grüneisen ratio, γ defined in Eq. (I-11), to describe the volume dependence of the Debye temperature, the ratio f_2/f_1 corresponding to volumes V_1 and V_2 is defined by

$$\frac{f_2}{f_1} = \exp\left[\frac{12RT\gamma}{k\Theta_1^2}\left(\frac{V_1 - V_2}{V_1}\right)\right]. \qquad \text{(II-12)}$$

Thus, the recoil free fraction increases with pressure. This was dramatically demonstrated by Stone et al.[48] in a Mössbauer study of Dy^{161} in gadolinium metal. A Mössbauer spectrum was not detected at atmospheric pressure, but a definite effect was observed at 35 kbars. Further evidence of the increase in the recoil-free fraction was observed by Panyushkin and Voronov[47] in pressure studies on Sn^{119}, where f increased by a factor of

three from 1 atmosphere to 110 kbars. The increase in f yields a value for the effective Debye temperature which in principle could be used to estimate an equation of state in the Debye approximation. Usually Debye temperatures determined in Mössbauer experiments differ significantly from those determined in thermal measurements. Thus, the equation of state would be qualitative at best.

An analogous application of the Mössbauer technique is the study of the pressure-temperature variation of the second-order Doppler effect, defined in Eq. (II-7). These results would yield heat capacities as a function of temperature and pressure. Preston et al.[62] have demonstrated the success of this application at 1 atmosphere in studies on iron over a wide temperature range.

The center of gravity of the Mössbauer spectrum is determined by the isomer shift and the second-order Doppler shift. It has been shown that the effect of pressure on the second-order Doppler shift is small,[44] so that a variation in the center of gravity with pressure is primarily due to changes in the electron density at the nucleus.

The pressure dependence of the internal field will be primarily dependent on the conduction electron contribution to the field. The core and orbital contributions are expected to be nearly independent of volume, because of their small spatial extent with respect to nearest neighbor distances. The compressibility of the conduction electron density is probably the same magnitude as the compressibility of the lattice. An increase in the conduction electron density results in an increase in the conduction electron contribution to the field. On the other hand, compression of the conduction electron density with respect to an approximately unchanged core can reduce the effectiveness of the

core polarization of the conduction electrons. These effects are compensating and consequently it is difficult to estimate the resultant volume variation of the internal field. This problem is further discussed below in light of the experimental results.

C. Experimental

1. General

The high pressure system was similar to that described in Section I. The hydraulic press used in the Mössbauer studies is capable of maintaining the load stable to within less than a kilobar over a period of several days. This feature was necessary, since individual experiments were run with counting periods up to seven days.

The primary problem in studying the Fe^{57} Mössbauer effect is the low energy of the gamma ray (14 keV). Since 14 keV radiation is attentuated by approximately 50% in passing through 30 mils of pyrophyllite, it becomes impractical to use an external source. Further problems arise from incomplete resolution of the 14 keV peak with respect to an intense 8 keV x-ray from iron, scattered radiation, and a certain percentage of 123 keV gammas which fall electronically into the 14 keV region. These effects tend to remain unchanged with pressure while the 14 keV radiation is severely attentuated with increase in pressure, thus reducing the observable Mössbauer effect.

Bridgman anvils with 1/4 in. tungsten carbide inserts were used. The anvil taper has been increased to 10 degrees to improve the counting geometry and to decrease the amount of scattered radiation observed at the detector. Pyrophyllite rings, 1/4 in. diameter, 1/32 in. wall, and 10 mils high, were used to contain the source in the pressure cell.

The sources were rings, 0.184 in. outside diameter, 0.163 in. inside diameter, and 0.007 in. high. These were prepared by electroplating Co^{57} onto a 1/3 segment of the ring. The rings were then annealed at 1000°C for 2-5 hours. Previously, Nicol[70] used a disc sample in high pressure Mössbauer studies, the Co^{57} being plated on the edge of the disc. These

samples were not always successful due to plating problems or because of excessive diffusion of the Co^{57} into the sample. The disc sample has the advantage of providing a large intensity of 14 keV radiation because of the localization of Co^{57} near the edge. In addition to reducing pressure gradients in the sample, the ring geometry has proved to combine several favorable features. The sample is rigid enough to handle with ease during electroplating, preliminary investigation of the Mössbauer spectrum, and in loading into the pressure cell. Also, the sample allows for sufficient localization of the plated material to prevent any difficulty in receiving sufficient 14 keV radiation through the pyrophyllite ring. All the samples were machined from rods of approximately the proper diameter or punched from 7-mil foil. The Co^{57} electroplating was performed by New England Nuclear Corporation. The amount of Co^{57} used varied from 2 to 16 millicuries depending on the particular experiment. All samples had a quoted purity of 99.999%.

The sample fits snuggly inside the gasket and the remaining volume is filled by a 7 mil high pyrophyllite disc. Ideally, silver chloride would be used inside the sample ring, but in several test runs with silver chloride the sample always extruded. The sample described is illustrated in Fig. II-5.

The average anvil pressure is measured in the same manner as described in Section I. Because the resistance of the metallic samples of the dimensions described is too small ($\sim 10^{-5}\Omega$) with respect to the contact resistances of the system ($\sim 10^{-4}\Omega$), an exact calibration of the sample pressure is impossible. Thus, the sample pressure is assumed to be equal to the average anvil pressure. The results of Nicol and Jura[45] on the pressure dependence of the isomer shift and internal field of Fe^{57}

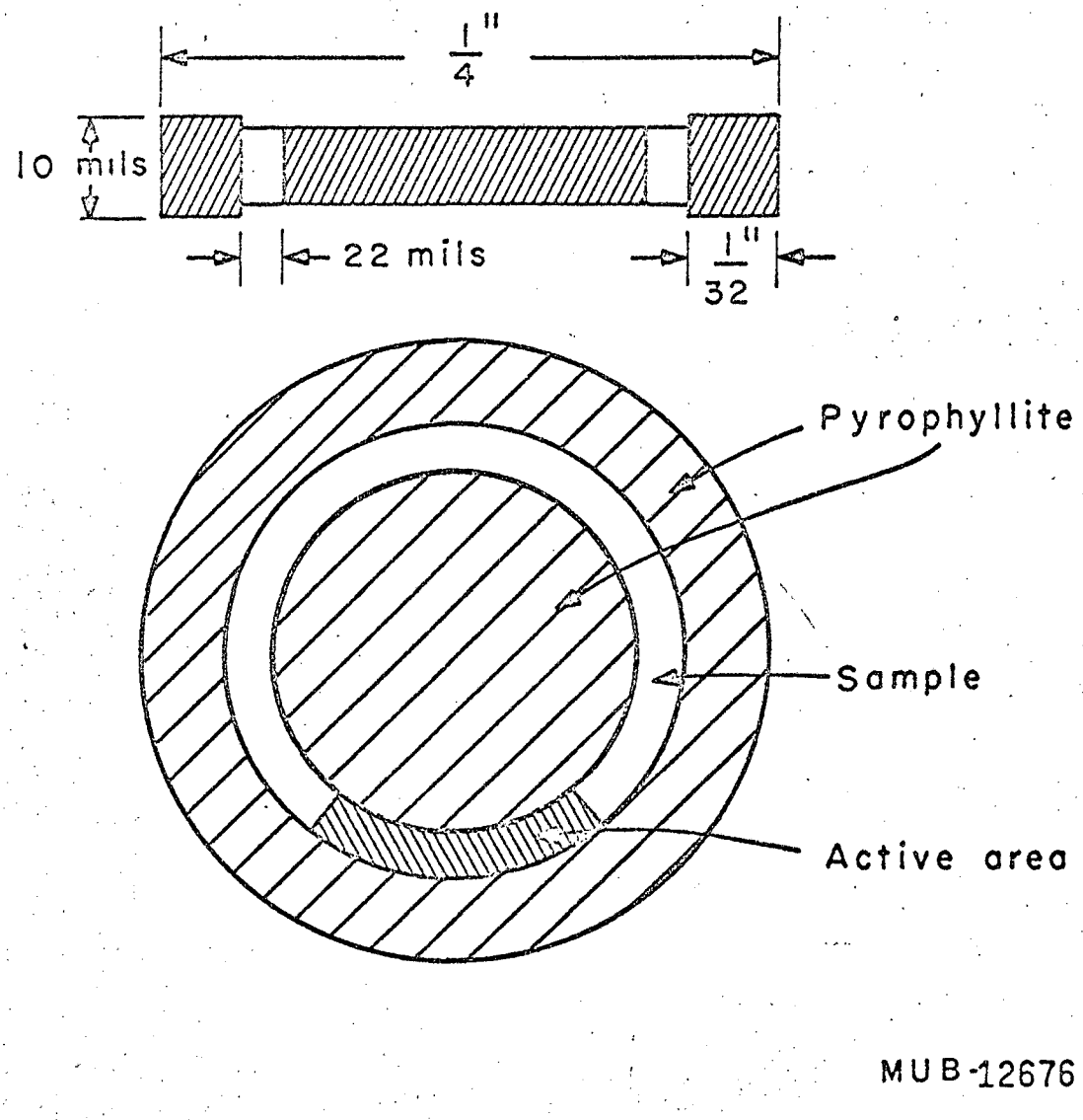

Fig. II-5 Sample geometry used in high pressure Mössbauer experiments.

in iron indicate that this assumption is probably correct. Using a disc sample as described above and assuming the average anvil pressure to be equal to the sample pressure, the pressure dependence of the internal field and isomer shift were equal to those observed in two independent experiments within the experimental errors.[46,71]

2. Mössbauer Spectrometer

There are two distinctly different techniques commonly used in Mössbauer spectroscopy. The first uses a constant velocity drive to sweep the required velocity interval. Thus, the Mössbauer spectrum is traced point by point by observing the intensity of radiation transmitted in a fixed time interval through an absorber moving at a constant velocity with respect to the source. The data obtained using this technique require corrections due to source decay and changes in the geometry of the counting system during a given experiment. Additional corrections are required in systems where line broadening exists at high velocities.

The second and most common technique utilizes a velocity sweep or loudspeaker drive to obtain the required velocities. The velocity interval is swept in a short time (~0.04 seconds), eliminating the necessity for making the corrections required in the constant velocity technique.

Both of the above techniques have been used in high pressure experiments in this laboratory.[45,48] Since the source must be contained in the pressure cell, there may be significant changes in the counting geometry during the course of an experiment as a result of material fatigue and creep in the anvils and sample. In addition, the counting system is always subject to some electronic drift. These considerations make the velocity sweep spectrometer more attractive in high pressure Mössbauer experiments.

Two types of velocity sweep spectrometers are in common use and both were used during the course of the work. These two methods are generally referred to as the "modulation mode" and the "time mode". Each uses a multichannel pulse height analyzer to record detector pulses during the short time used for the velocity sweep. Since the counting system and the drive assembly are common to each apparatus they will be described first.

a. Counting System. The counting system employed in this work has been described in detail previously[70] and it will be discussed only briefly here. A NaI(Tl) scintillation crystal 1 in. in diameter and 1 mm. thick (supplied by Harshaw Chemical Company) is used to detect the 14 keV radiation. The crystal is mounted on the face of a Dumont 5292 phototube, selected so that the noise level corresponds to energies somewhat below the 8 keV x-ray of iron. Phototube power is supplied by a Carad H-V power supply. A linear amplifier (LRL MOD VI 3x9499) amplifies the phototube output and a single channel analyzer (LRL 4x69537) separates the 14 keV radiation from the full spectrum. It is noted that the 14 keV peak is not fully resolved from the 8 keV peak and a certain amount of higher energy radiation coming from the intense 123 keV peak falls electronically into the 14 keV region. A Victoreen 400 channel pulse height analyzer is used to display the γ-ray spectrum, the gated output of the single channel analyzer, and ultimately the Mössbauer spectrum.

b. Drive Assembly. The drive assembly consists of three parts; the absorber, the velocity transducer, and the voice coil. The system is illustrated in Fig. II-6, the scale being altered to show the primary features of the system. The capsule is similar to that used by Nicol[70] with the exception of the mechanical support. Previously the moving

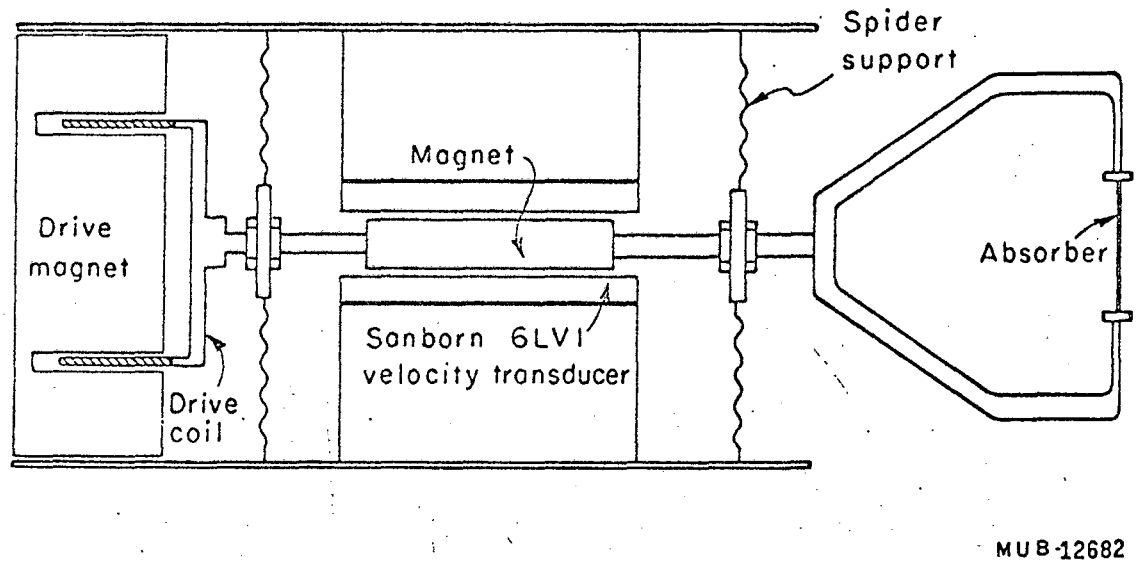

Fig. II-6 Mössbauer drive assembly.

assembly had been supported by a set of six adjustable wires. Because of fatigue in the wires and difficulty in obtaining equal tension in the six wires, the resonant frequency of the system tends to drift with time. These drifts result in a change of the velocity scale, thus requiring frequent calibration of the system. This suspension system is also sensitive to surrounding vibrations that result in significant distortion in the motion of the absorber. These difficulties led to the use of a different support system. The wire supports were replaced by fibrous spider supports, which were epoxied to collars which fit snuggly inside the capsule. These proved to be much superior, needing no adjustment and being considerably more stable with respect to vibrations in the laboratory.

The drive coil provides an acceleration proportional to the current passing through it, while the velocity transducer provides an output voltage proportional to the instantaneous velocity of the moving assembly. The linearity of the voltage with respect to the velocity is approximately 1% for a displacement of 1 inch. The assembly is usually operated at frequencies from 12 to 35 cps.

The absorber used in all the high pressure runs was an 0.7 mil stainless steel foil made from iron enriched to 91.2% Fe^{57}. The chemical composition of the foil is 9.6% nickel, 18.4% chromium, 0.15% carbon, and 71.8% iron. A 1-inch diameter section of the foil is mounted in a holder which is rigidly attached to the yoke of the moving assembly. This absorber provided a broad unsplit absorption line. This broad absorption line is not favorable for precise measurement of the hyperfine splitting and isomer shift, but because the absorber provides a very intense spectrum, it is necessary in the high pressure runs where the ratio of 14 keV to background radiation decreases sharply.

A second absorber was used for preliminary studies at atmospheric pressure. This absorber, sodium ferrocynanide enriched in Fe^{57} and dispersed in acrylic plastic, provides a single narrow line close to the natural linewidth.

c. Modulation Mode. In the modulation mode, the transducer output, which is proportional to the instantaneous velocity of the absorber, is used to modulate the detector pulses from the single channel analyzer in such a way that their pulse height is proportional to the velocity. These pulses are then handled by a pulse-height analyzer operating in the normal analog to digital conversion mode, such that channel number is a linear function of velocity. The CRT of the analyzer will display a true picture of the velocity spectrum only if the system spent equal times at each velocity interval during the measurement. This requirement is fulfilled only if the analyzer dead time is constant for all channels and the absorber has a linear velocity wave form. Thus, for accurate measurements it is necessary to determine the time spent in each velocity interval by observing a non-resonant spectrum under the same conditions used in determining the actual Mössbauer spectrum. A Mössbauer spectrometer operating in the modulation mode has been constructed previously in this laboratory[70] and was used in this work.

Briefly, the voice coil is driven sinusoidally through a matching transformer by a Krohn-Hite Model 446 oscillator. The output of the velocity transducer is amplified with a Kintel Model 111 amplifier and applied to the input of a velocity-to-pulse-height converter (VPHC, LRL 4x9021). The output of the Kintel amplifier is monitored with a Tektronix Type Z differential amplifier and Tektronix 545 oscilloscope. This permits the velocity oscillations to be controlled to within 0.2% assuming the gain

of the amplifier remains constant. The VPHC also receives square pulses from the single channel analyzer corresponding to 14 keV radiation transmitted through the absorber. The SCA pulses are modulated by the transducer voltage, and accumulated by the pulse height analyzer. The analyzer data is then punched out on paper tape for computer data reduction and curve fitting. Since the absorber velocity varies sinusoidally with time, the spectrum must be normalized as described above. The complete system is illustrated in block form in Fig. II-7.

The disadvantages of this system are primarily the velocity drift and the increased statistical error resulting from the spectrum normalization. These problems are particularly important when the intensity of the observed lines is very low which is commonly the case in high pressure runs. These considerations led to the final use of a time mode Mössbauer spectrometer in the later stages of the work.

d. Time Mode. In this technique the pulse height analyzer is operated in a multiscalar or time mode, in which the channels of the analyzer are sequentially opened and closed by an external signal. During the open time the channel acts as a simple scalar, accepting pulses from the single channel analyzer. The Mössbauer spectrum may be observed if the absorber velocity is kept in synchronization with the scalar advance pulses. This is accomplished by using a tuning fork oscillator as a primary frequency standard to control the timing of the scalar advance pulses, the velocity wave, and start pulses which re-initialize the analyzer when all channels have been scanned. The oscillator operates at a frequency of 20 kc and is stable to within 0.02% over a temperature range of 35°C. The primary frequency may be divided by two to allow either a 10 or 20 kc scalar advance pulse. The scalar advance frequency is further divided by the

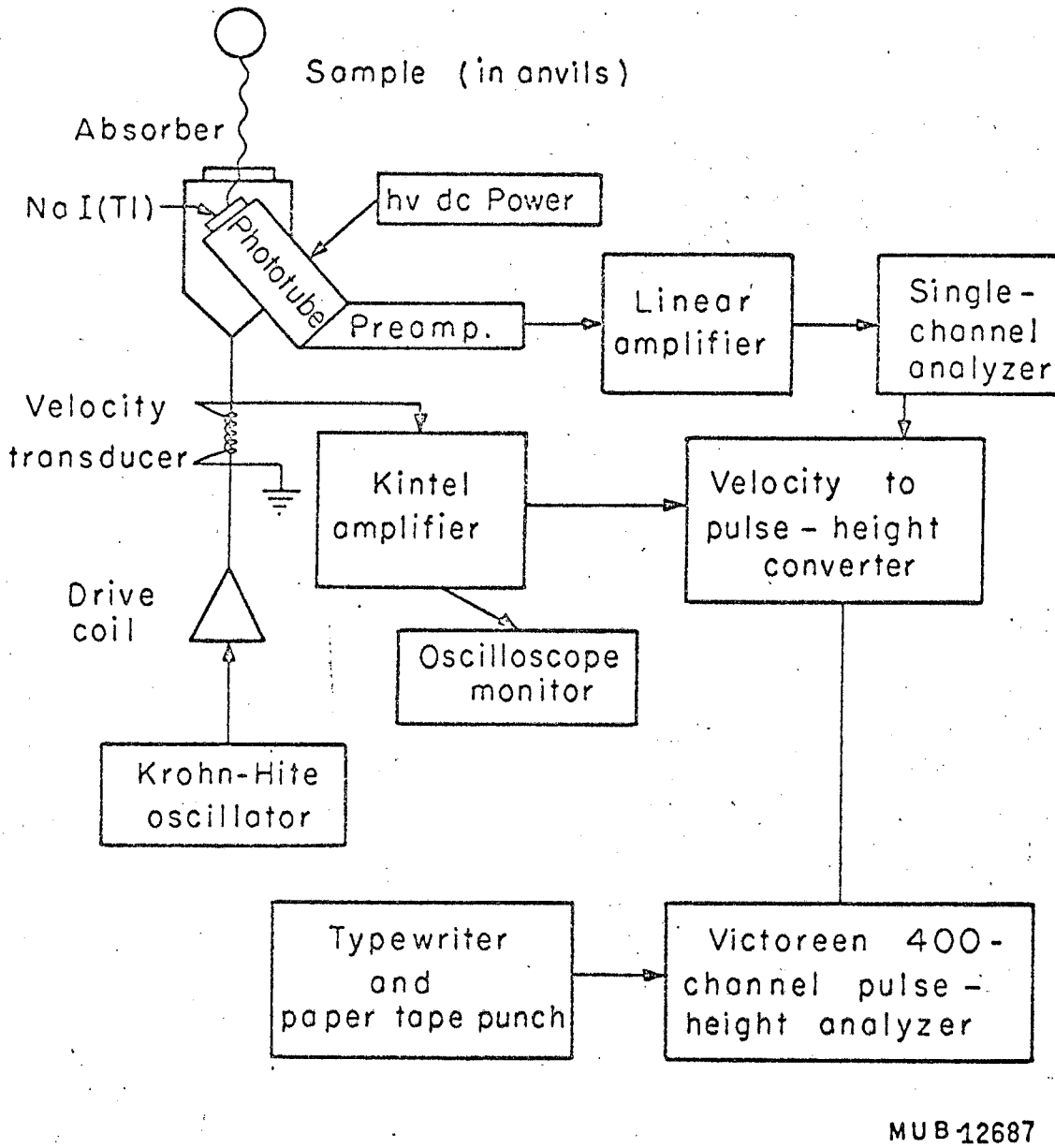

Fig. II-7 Block diagram of Mössbauer spectrometer (modulation mode).

number of channels to produce a 25 cps square-wave start pulse. This square-wave is then integrated to produce a 25 cps triangle wave which is used to control a closed-loop velocity feedback drive, producing a linear relationship between channel number and velocity. This system has been developed and described in some detail by Zane.[72] Ideally, a square wave accelerating force would be used to drive the loudspeaker coil, but experimentally it was necessary to add a small parabolic correction term to the square wave. This correction term compensates for the simple harmonic nature of the moving assembly coupled to the spider supports. The parabolic wave is easily obtained by integration of the triangle wave and is automatically synchronized with the rest of the system. The motion is quite linear except at the vertices. The vertices are not important since they may be made to fall outside the velocity interval of interest. The deviation from linearity has been estimated at less than 1% by comparing the observed splittings of Fe^{57} in iron with literature values.[73]

It is noted that a start pulse is generated at the frequency of the velocity wave, 25 cps. This results in the accumulation of two Mössbauer spectra if the scalar advance operates at 10 kc or just one spectrum if operated at 20 kc (for a 400 channel analyzer). This system has then been applied in the later experiments to be described. A block diagram of the complete system is illustrated in Fig. II-8.

3. Data Analysis

Rapid data analysis is facilitated by the use of high-speed computers. More important, computers allow one to use minimization techniques to determine the parameters of the Mössbauer spectra, such as line positions, intensities and linewidths. Since there are 14 variable parameters

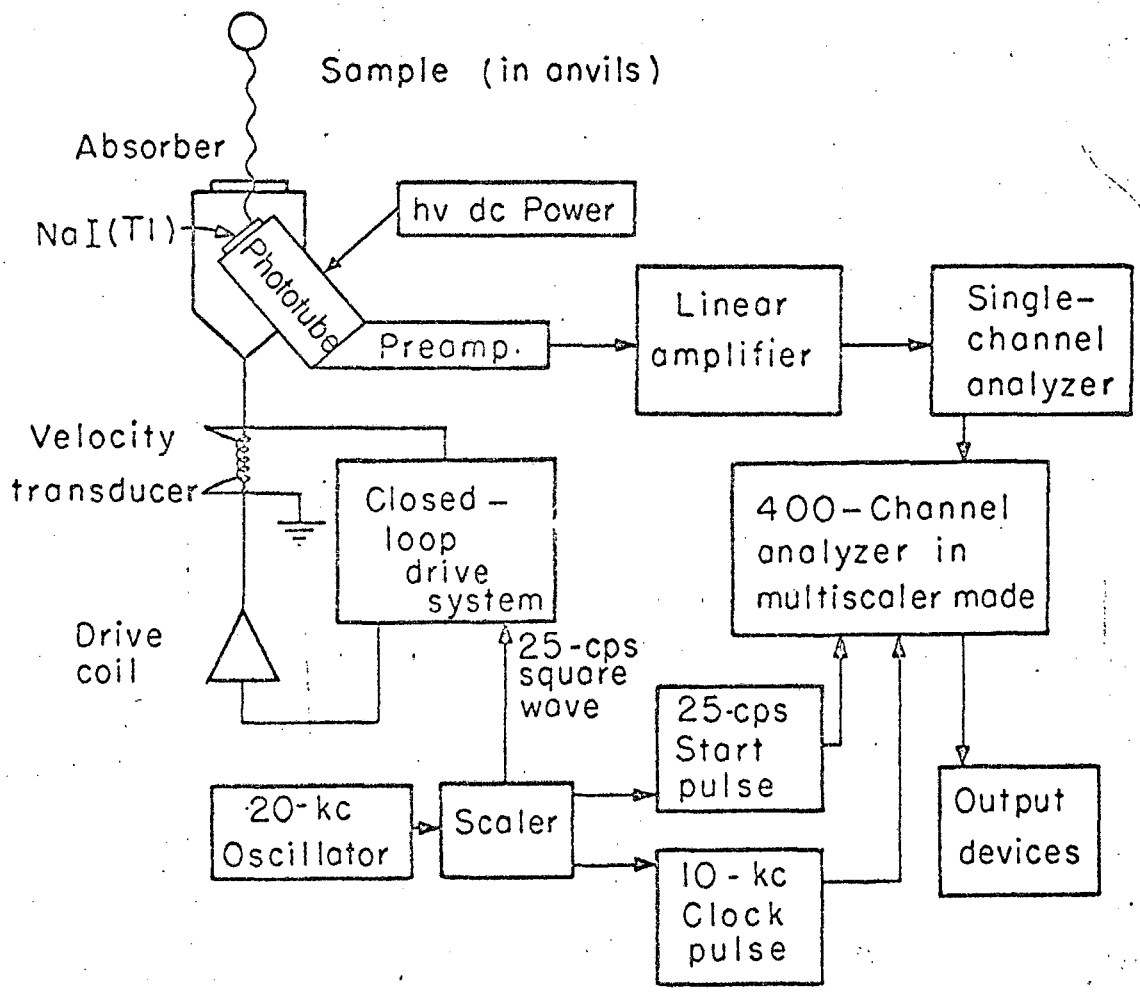

MUB-12671

Fig. II-8 Block diagram of Mössbauer spectrometer (time mode).

associated with a six line Mössbauer spectrum, it is clearly impractical to obtain a least squares analysis of the spectrum by hand calculation. Immediate application of the data to computer analysis was facilitated by the addition of a Tally paper tape punch as a digital output device of the pulse height analyzer. Using the Chemistry Department's SDS 910 computer or the similar DDP-24 located at the laboratory computer center, data reduction could be performed within minutes after a spectrum was obtained. Such rapid analysis is not essential in most applications but can provide an immediate answer when the next step in an experiment is questionable.

Because of the overlap of the broad lines obtained with the stainless steel absorber, it is necessary to separate the contributions of the individual lines in order to determine the parameters of the Mössbauer spectrum. This is a tedious task when performed by hand. For each run, the spectrum was fit with six Lorentzian lines by means of a least squares analysis performed with a program developed for use on either an IBM-7094 or CDC-6600 computer. The computer program permits the application of various constraints during the calculation. For instance, the value of any parameter may be fixed, or any linear relationships among the parameters may be specified. Thus, the computer can be required to make the best fit with the condition that the separations between lines 1 and 2, 2 and 3, 4 and 5, 5 and 6 be equal. This constraint corresponds to the situation expected for cubic symmetry of the source lattice assuming the use of a single line absorber. In the analysis of the data reported here, constraints were not ordinarily imposed unless the resolution was so poor as to require them in order that a fit could be obtained.

The center of gravity of the spectrum was calculated from the resultant line positions and intensities. The internal field was determined from the positions of the two outer lines and the quadrupole splitting parameter was determined from the positions of the four outer lines. The velocity scale is calibrated by determining the Fe^{57} Mössbauer effect in iron which has been determined accurately in previous experiments. The splitting of the two outer lines is 10.64 mm/sec.[73] A typical analysis of a spectrum is shown in Fig. II-9 where the spectrum has been decomposed by least squares analysis.

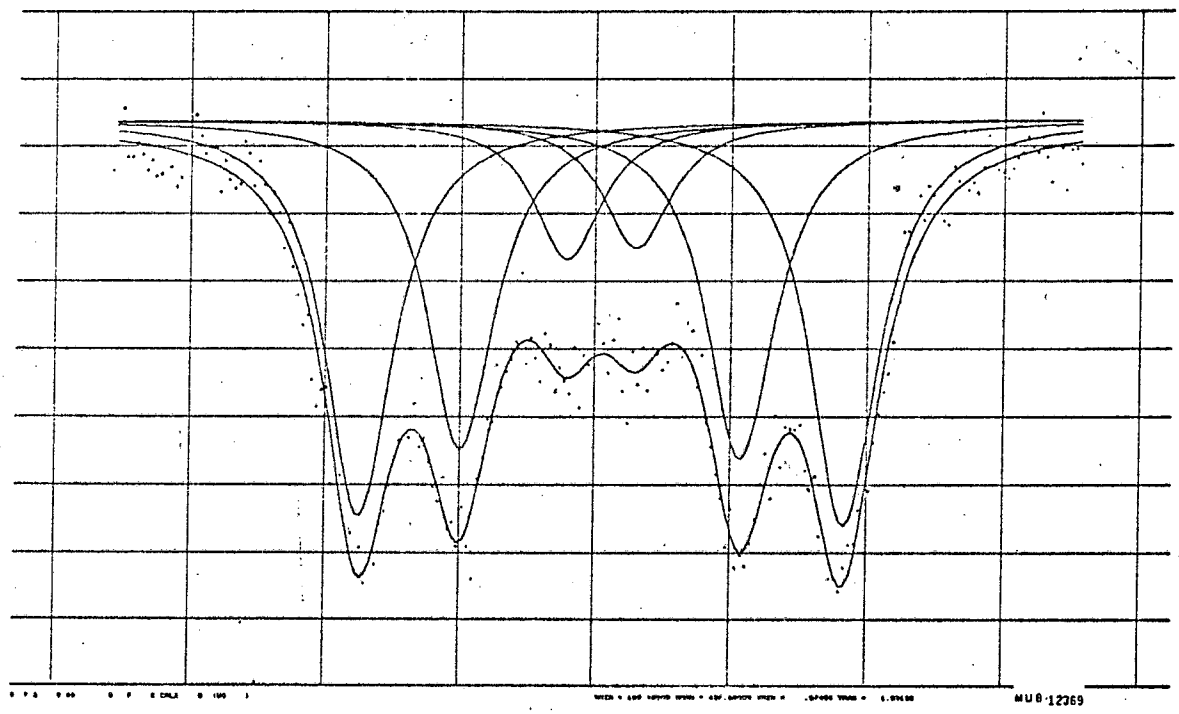

Fig. II-9 Mössbauer spectrum of Fe^{57} in iron at 1 atmosphere. The spectrum is decomposed into 6 Lorentzians by least squares analysis.

D. Iron Experiment

1. Introduction

Iron is a material of great theoretical and practical interest and Fe^{57} is one of the best isotopes for studying the Mössbauer effect. The Mössbauer spectrum of Fe^{57} in iron metal has been studied over a wide range of experimental conditions. These experiments have answered a number of questions about the interactions of the nucleus with the surrounding electrons and the relationship of these interactions to the bulk properties of solids. The present experiment is concerned primarily with the study of the high pressure phase transition in iron metal.

At atmospheric pressure and room-temperature iron has the body-centered-cubic structure (bcc, α-iron).[74] It is ferromagnetic up to the Curie temperature 770°C.[74] Patrick[75] found the Curie temperature to be nearly independent of pressure up to 10 kbars. At 910°C it transforms to a face-centered-cubic phase (fcc, γ-iron).[76] Shockwave[77,78] and electrical resistance measurements[79,80] have revealed a phase transition at 130 kbars at 25°C. The phase boundary between α-iron and the high pressure phase has been traced as a function of pressure and appears to meet the α-γ phase boundary in a triple point.[78,81-84] The phase diagram is illustrated in Fig. II-10. X-ray diffraction measurements at high pressure[85,86] have shown the high pressure phase to have an hexagonal close-packed (hcp) structure. In static high pressure experiments the transition is very sluggish, sometimes extending over a range of 80 kbars. The sluggishness of the transition may result from a high activation energy for the process or because of a small free energy difference between the two phases. Stark and Jura[80] have applied a current-pulse technique to iron and obtained a reasonably

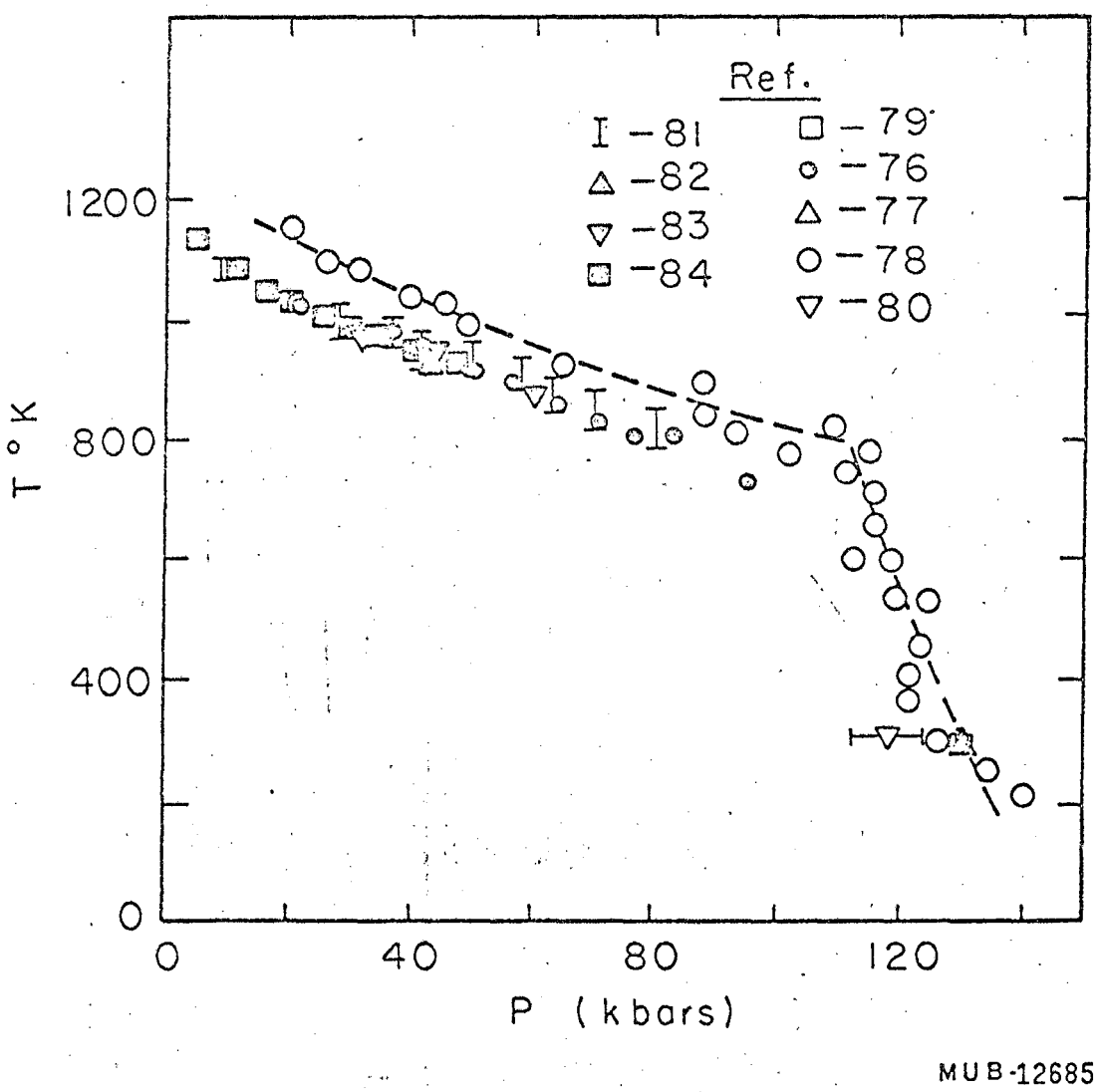

Fig. II-10 Phase diagram of iron.

sharp transformation to the hexagonal phase at 118±6 kbars. This method is based on the negative slope of the T-P phase line. Therefore, raising the temperature at constant pressure near the phase boundary results in a partial transformation of the material to the high pressure phase. Then, if one phase grows at the expense of the other, it is probably the thermodynamically stable phase at that temperature.

Three Mössbauer experiments on Fe^{57} in iron have been reported. Pound et al.[44] measured the isomer shift up to a hydrostatically applied pressure of 3 kbar. The relative change in the shift with pressure is given by

$$\frac{d(IS)}{dP} = -7.98\times10^{-5}(\text{cm/sec})\text{kbar}^{-1} \qquad \text{(II-13)}$$

or in terms of the relative volume change

$$\frac{d(IS)}{d(V/V_0)} = 0.134 \text{ cm/sec.} \qquad \text{(II-14)}$$

A second experiment was performed in this laboratory by Nicol and Jura.[45] In this work, the isomer shift and internal magnetic field were studied up to 140 kbars. At 140 kbars a seventh line was superimposed on the normal six line spectrum of α-iron. The seventh line was attributed to a partial transformation of the α-iron to the hexagonal phase. Further attempts to study the spectrum above 140 kbars were unsuccessful. In the most recent iron experiment, Pipkorn et al.[46] studied the iron spectrum to a maximum pressure of 240 kbars. A seventh line appeared at 130 kbars and increased in intensity with increasing pressure. Correspondingly, the six line spectrum slowly disappeared. A pressure of 170-200 kbars was needed to transform most of the source to the hexagonal phase.

The results of the above experiments are all in agreement within

the experimental errors. These data are compiled and illustrated in Figs. II-11 and II-12. An independent check of the internal field measurements is provided by the nuclear magnetic resonance results of Litster and Benedek[71] up to 65 kbars. The variation of the internal field with pressure is given by

$$\frac{d\ln H}{dP} = -1.69\times10^{-4}\ \text{kbar}^{-1}. \qquad \text{(II-15)}$$

This results is illustrated in Fig. II-12. The magnitude of the observed isomer shift in α-iron corresponds to a scaling of the 4s wave function with volume.[46] In other words, the increase in the 4s density is proportional to the decrease in volume. This may be written analytically

$$\frac{d\ln[\psi_{4s}(0)]^2}{d\ln V} = -1. \qquad \text{(II-16)}$$

The shift of the hcp phase relative to the α-phase is -0.17 mm/sec.[46] This is much larger than is expected on the basis of the volume change (2.2%). Pipkorn et al.[46] have discussed the magnitude of the observed shift in terms of a difference in band structure of the two phases. The single line of the hcp phase is understood if there is no aligned localized magnetic moment on the iron atoms. The four-fold increase in the electrical resistance observed upon transformation to the hcp phase[79] suggests a major electronic rearrangement which may prevent ferromagnetic ordering in the high pressure phase. It is noted that unsplit Fe^{57} Mössbauer spectra have been observed in ferromagnetic alloys[87] and for Fe^{57} in antiferromagnetic chromium.[88] Thus, the single line does not necessarily imply that the hcp phase of iron is paramagnetic.

The present experiment was stimulated by the uncertainty in the nature of the high pressure phase of iron, caused by the extreme

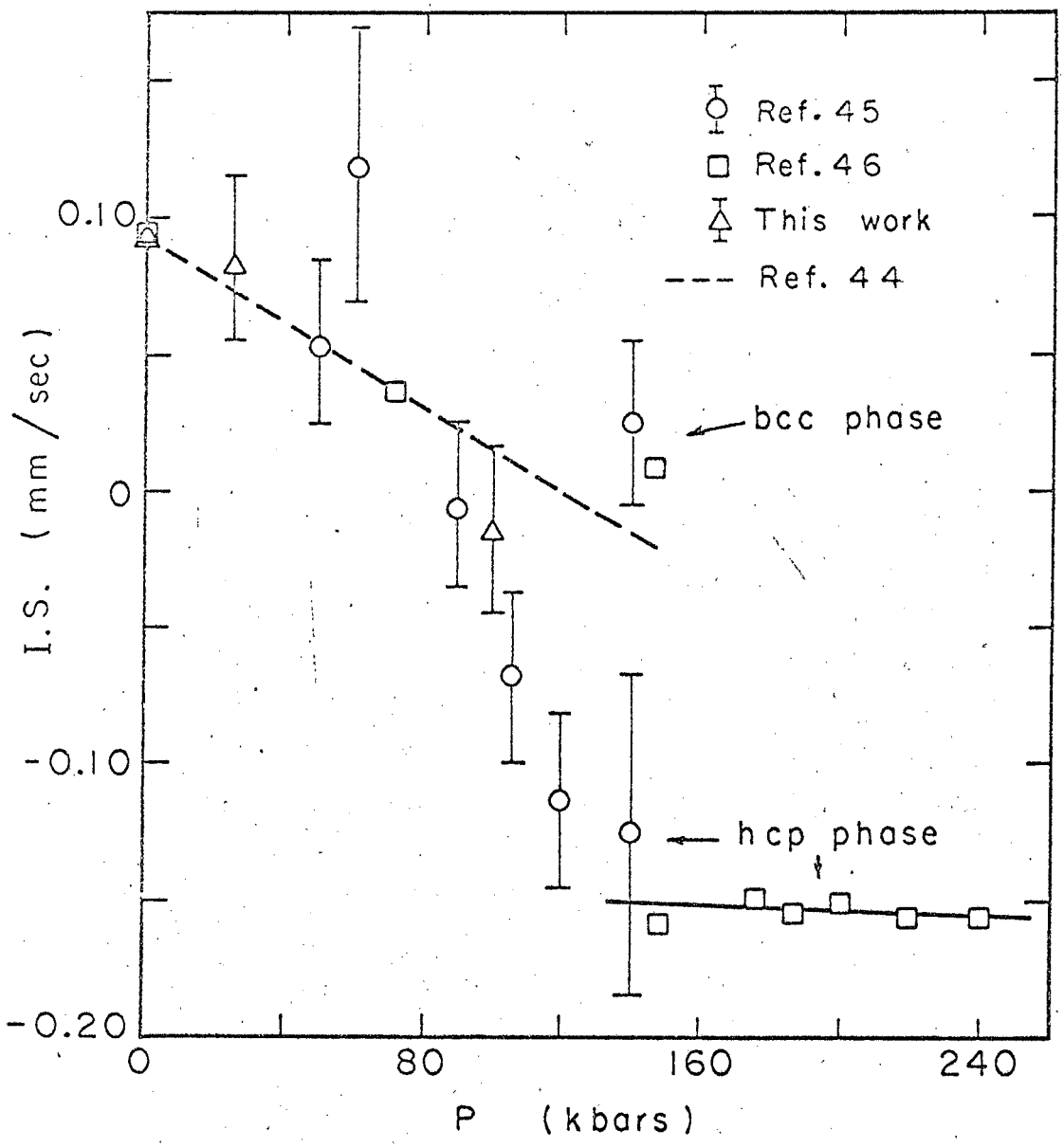

MUB-12684

Fig. II-11 The variation of the isomer shift of Fe^{57} in iron with pressure.

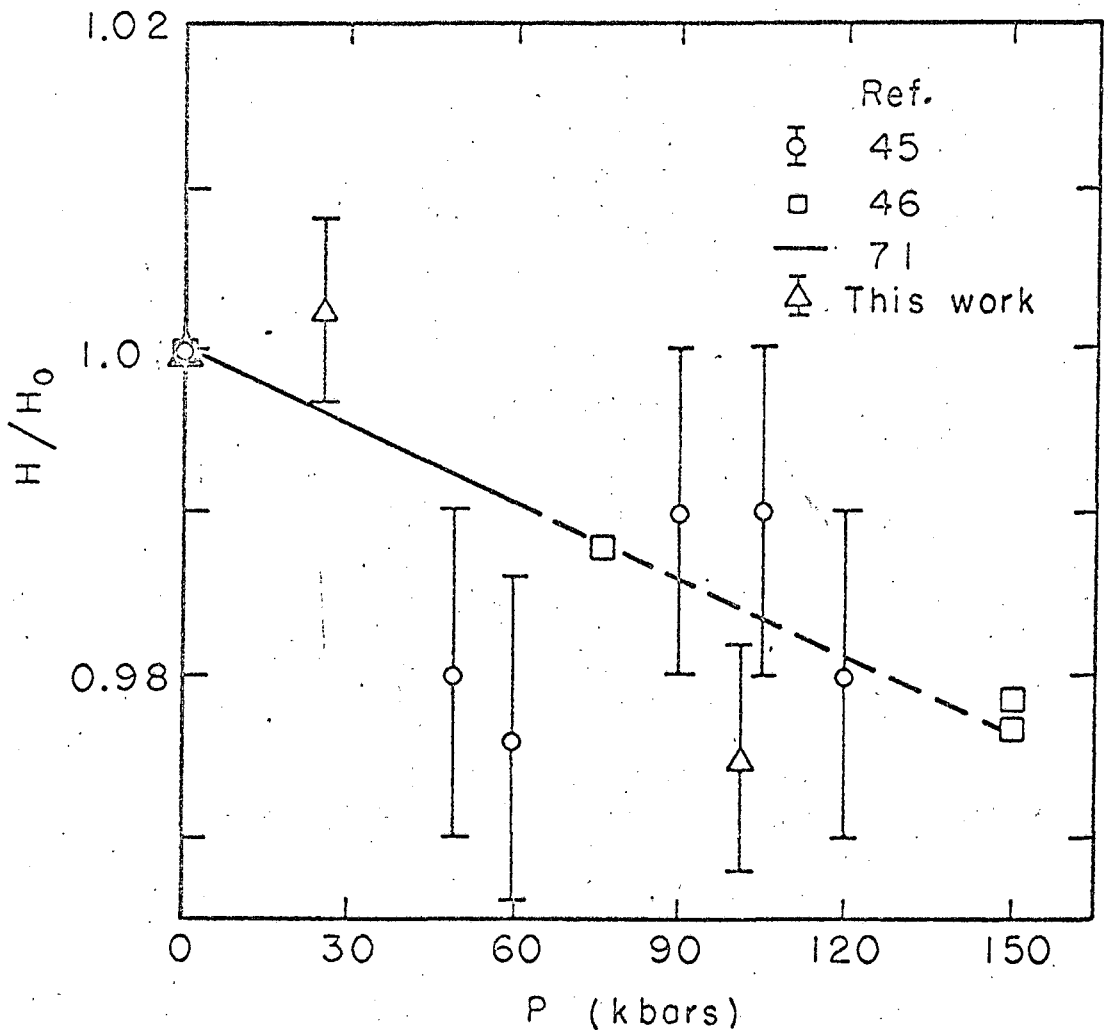

MUB-12673

Fig. II-12 The variation of the internal magnetic field of Fe^{57} in iron with pressure. The dashed line is an extrapolation of the results of Litster and Benedek.[71]

sluggishness of the phase transition. Utilizing the pulse technique of Stark and Jura,[80] it is feasible to obtain a complete transformation of the iron to the hcp phase at a pressure of 120 kbars.

2. Experimental

The Mössbauer spectrometer and sample assembly are described above. The source used in this work was an iron ring with 16 millicuries of Co^{57} electroplated and diffused into the ring. The pulsing system is similar to that described by Stark and Jura.[80] Because the Mössbauer sample makes direct contact with the anvils, the heat leak away from the sample is so large the sample temperature cannot be increased to a high value. Also, the sample resistance of 10^{-5} ohms is dominated by a contact resistance between the sample and anvils of approximately 10^{-4} ohms. Therefore, most of the heating occurs at the contacts. Using three 12-volt storage batteries as a power source, a 1000 amp pulse could be maintained for several seconds across the anvils. Alternatively, up to 20 short duration pulses of the same magnitude could be obtained.

Several Mössbauer spectra were obtained up to a maximum pressure of 140 kbars. The spectra which have bearing on the following discussion are reproduced in Figs. II-13 and II-14. These spectra have been constructed by averaging the raw data over nine adjacent channels to reduce the effect of statistical fluctuations in visual examination of the data.

3. Results and Discussion

The spectra illustrated in Figs. II-13 a,b,c and d were obtained at 1 atm, 25, 100, and 120 kbars, respectively. At 120 kbars the intensity of the outer lines is less than 1%. Because of the low counting rate encountered above 100 kbars (1000 counts/channel/hour), approximately five days were required to obtain each of the illustrated spectra.

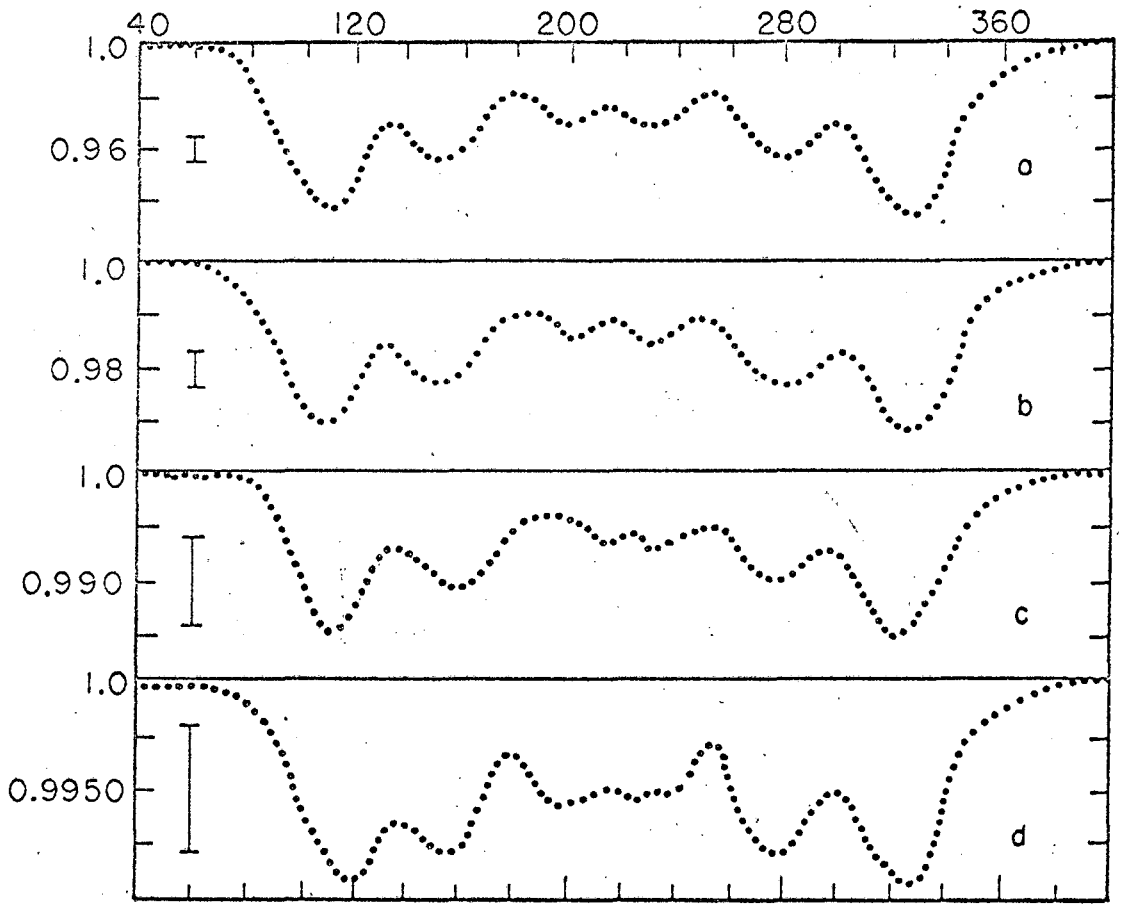

MUB-12677

Fig. II-13 Mössbauer spectra of iron: a) 1 atmosphere, b) 25 kbars, c) 100 kbars, d) 120 kbars. Flags indicate statistical error in raw data.

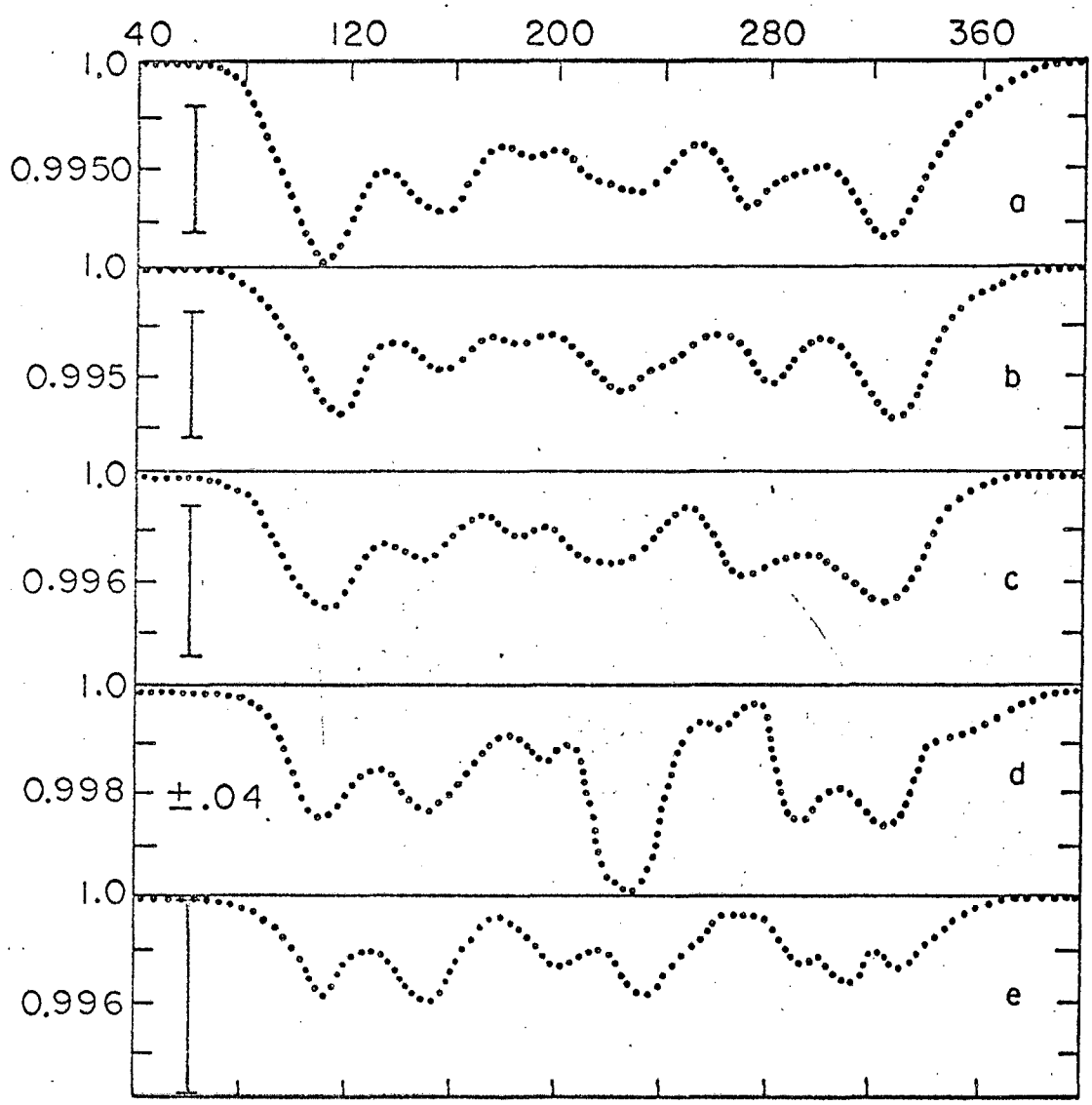

MUB-12675

Fig. II-14 Mössbauer spectra of iron: a) 120 kbars (first pulse) b) 120 kbars (second pulse) c) 130 kbars (first pulse) d) 120 kbars (48 hours after decompression from 140 kbars) e) 120 kbars (72 hours after decompression from 140 kbars).

The isomer shift and internal field were calculated at 1 atm, 25 and 100 kbars. These were in agreement with previous results and given earlier in Figs. II-11 and II-12.

The spectra obtained after pulsing the iron sample are given in Fig. II-14. After pulsing at 120 kbars (Figs. II-14a and b), it was evident that the iron was being slowly transformed to the high pressure phase. There is a definite increase in the intensity near zero velocity (~ channel 220) with a corresponding decrease in the intensity of the six-line spectrum of α-iron. Because the transformation rate was slow, the pressure was increased to 130 kbars. The intensities (Fig. II-14c) were again extremely low and a full transformation was not obtained. At 140 kbars the spectrum could not be separated from the noise level during a counting period of seven days. The pressure was then decreased to 120 kbars. Figures II-14d and e illustrate spectra obtained after 48 and 72 hour counting periods. The intensities were lower than in earlier runs at 120 kbars, presumably because of deformation of the anvils at the higher pressures. Although the statistical errors are large, the 48 hour spectrum shows a strong central line. After 72 hours, the central line decreased in intensity with a corresponding increase in the outer lines. A second attempt to study the spectrum after decompression from 140 kbars proved unsuccessful, and the experiment was terminated.

The estimated rate constant, k, for the transformation of hcp-iron to α-iron at 120 kbars is 0.012 hrs^{-1} where k is given by the first order rate equation,

$$\frac{C_2}{C_1} = e^{-k(t_2-t_1)} \qquad \text{(II-17)}$$

and C_2/C_1 is the relative concentration of hcp-iron at times t_2 and t_1. The initial intensity at time zero calculated from Eq. (II-17) is 0.7%.

4. Conclusions

Unfortunately, the severe attenuation of the 14 keV Mössbauer radiation above 100 kbars prevented the attainment of the initial goals of this work. The results are qualitative at best, but they point the way to further experiments. It seems definite that the high pressure phase of iron is characterized by a single line spectrum, confirming the results and conclusions of Pipkorn et al.[46] The interesting aspect of the present work is the ability to study the kinetics of the high pressure phase transition. The Mössbauer technique has been previously applied to kinetic studies,[89] but this is the first use of Mössbauer data in high pressure kinetic studies. To date, very little data are available on the kinetics of high pressure phase transformations. The activation energy can be found by studying the temperature dependence of the iron transition. Additionally, the pressure dependence of the rate constant may be compared with present kinetic theory.[90] These data would be extremely useful in furthering our understanding of high pressure phenomena.

The problem of the low intensity of transmitted 14 keV radiation with respect to background radiation may be partially solved by the use of the recently developed solid state detector systems. Lithium-drifted silicon detectors have proven to be highly successful in studying low energy gamma ray spectra. It would certainly be worthwhile to make further studies of the iron phase transformation with an improved detector system.

E. Nickel Experiment

1. Introduction

Mössbauer studies of Fe^{57} in iron have illustrated the usefullness of the Mössbauer effect in solid state physics. By studying the volume dependence of the internal field and isomer shift of Fe^{57} in different environments, we may further understand the origin and relationship of these nuclear parameters to the bulk properties of solids. Thus, the pressure dependence of the Fe^{57} Mössbauer effect in nickel metal has been carefully studied to a maximum pressure of 80 kbars.

Nickel metal has the face-centered-cubic structure at 1 atmosphere and room temperature.[74] It is ferromagnetic up to the Curie temperature 360°C.[74] Patrick[75] found the Curie temperature of nickel to increase by +0.35°C/kbar up to a pressure of 8 kbars. Other high pressure investigations have revealed discontinuities in the slopes of the pressure coefficient of resistivity $(1/P)(\Delta R/Ro)$ versus pressure[22] and in the volume versus pressure curves.[91] These results are reproduced in Fig. II-15. A discontinuous change in the slope of the pressure-volume curve is usually characteristic of a second order phase transition, such as the Curie or Néel point in magnetic materials. Similar discontinuities have been observed in other transition metals, notably chromium which is antiferromagnetic below 38°C.[22] Lawson[22] has pointed out the possibility that resistivity kinks and compressibility anomalies may be related to the complicated band structure of transition metals. Since the pressure-resistivity anomaly in chromium is related to the antiferromagnetic-paramagnetic transition,[92] the possibility of a second order phase transition in nickel is not ruled out.

The Mössbauer effect of Fe^{57} in nickel metal has been studied up to

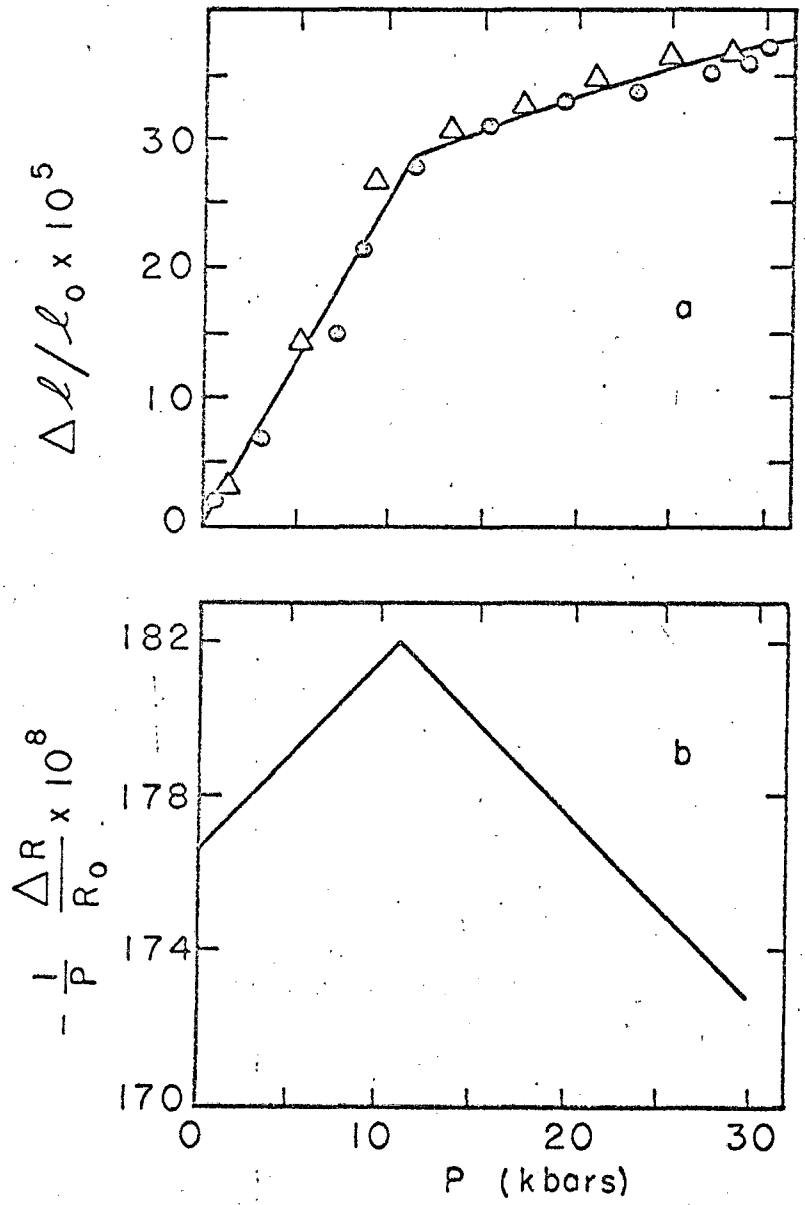

MUB-12680

Fig. II-15 a) Differential change of length of nickel with pressure (after Bridgman[91]). b) Pressure coefficient of resistance of nickel as a function of pressure (after Lawson[22]).

a pressure of 250 kbars.[93] This study was primarily concerned with the very high pressure region above 60 kbars. The internal field and isomer shift vary slowly with pressure. These results are compared with those of the present work in Sec. II-3. NMR studies of Ni^{61} in nickel show a large increase in the internal field with pressure up to 7 kbars.[94] The relative increase in the hyperfine field is given by

$$\frac{d\ln H}{dP} = + 8.81\times10^{-4}\ \text{kbar}^{-1} \qquad \text{(II-18)}$$

The magnitude of the internal magnetic field at 0°K in nickel metal is -90 kgauss,[95] compared with a value of -342 kilogauss for iron.[56] The value of H for Fe^{57} in nickel is -280 kgauss.[66] Table II-I summarizes the data on internal fields for the pure metals and dilute alloys of Fe, Co, and Ni. It is noted that in each case the field at the iron nucleus in a given metal is in every case larger than the field at the host lattice nucleus. This suggests that the field at an iron nucleus is due largely to its own electrons and depends only slightly on the host magnetization. If it is assumed that the core contribution to the internal field at the Fe^{57} nucleus is independent of the host lattice, and the conduction electron contribution is independent of the impurity atom, the conduction electron contribution to the total field may be estimated by observing the internal field at a diamagnetic atom in the host. The internal fields at the Sn^{119} nucleus in iron, cobalt, and nickel are -88, -26.5, and +16.5 kgauss, respectively.[101] Adding to these values the core contributions of the Fe^{57} atoms (-280 kgauss), containing the core polarization and orbital terms, the results values for the internal fields at Fe^{57} nuclei in iron, cobalt, and nickel are -368, -306, and -264 kgauss, respectively. These values are in rough agreement with the observed

Table III-1 Magnetic fields in units of 10^5 gauss at transition metal nuclei located in transition metals

Nuclei at which field is measured	Lattice Atoms		
	Fe	Co	Ni
Fe	3.42[a]	3.12[b]	2.80[c]
Co	3.20[d]	2.20[d]	1.11[f]
		2.134[e]	
Ni	2.52[g]	2.03[g]	0.90[h]

a. Ref. 56
b. Ref. 96
c. Ref. 66
d. Ref. 97
e. Ref. 98
f. Ref. 99
g. Ref. 100
h. Ref. 95

field in these metals. Evidence that the conduction electron contribution is nearly independent of the impurity atom is found in results on the pressure dependence of internal fields in dilute alloys. The pressure dependence of the internal field should primarily reflect changes in the conduction electron contribution to the field. These data have been collected and tabulated in Table II-II. There is a distinct grouping of coefficients according to host.

2. Experimental

The high pressure Mössbauer apparatus has been described earlier. Both of the described spectrometers were used in the investigation. The experimental results on the pressure dependence of the isomer shift and internal field are compiled in Fig. II-16 and II-17, respectively. Run 1 was performed on a nickel source with 8-millicuries of Co^{57} electroplated onto the nickel ring. Because of the apparent peak in the internal field-pressure curve at 10 kbars, a second 2-millicurie source was studied carefully up to 70 kbars. Again the peak was present in the 10 kbar region. The variation of the isomer shift with pressure is in good agreement with Drickamer.[93] Also, the internal field at 60 kbars agrees with the results of Drickamer within the experimental error. The initial rate of increase in the internal field was calculated by fitting the data from 1 atm to 12.5 kbars to a straight line by least squares analysis. The pressure coefficient of the field is given by

$$\frac{d\ln H}{dP} = +\ 10.2\times10^{-7}\ \text{bar}^{-1}. \qquad \text{(II-19)}$$

The value of the internal field at 1 atm is 270±5 kgauss. Similarly, a least squares fit of the isomer shift data yields

$$\frac{d(IS)}{dP} = -4.15\times10^{-5}\ (\text{cm/sec})\ \text{kbar}^{-1} \qquad \text{(II-20)}$$

Table II-II The pressure dependence of the internal field H in transition metal systems

Nucleus	Host	$(d\ln H/dP)\times 10^7$ bar^{-1}
Ni^{61}	Ni	+8.81[a]
Co^{59}	Ni	+13.8 [a]
Fe^{57}	Ni	+10.2 [b]
Co^{59}	Co	+6.1 [c]
Fe^{57}	Co	+6 [d]
Cu^{63}	Fe	-3.0 [e]
Co^{59}	Fe	+1.6 [e]
Fe^{57}	Fe	-1.69[f]

a. Ref. 94

b. This work

c. Ref. 64

d. Preliminary results of author

e. Ref. 102

f. Ref. 71

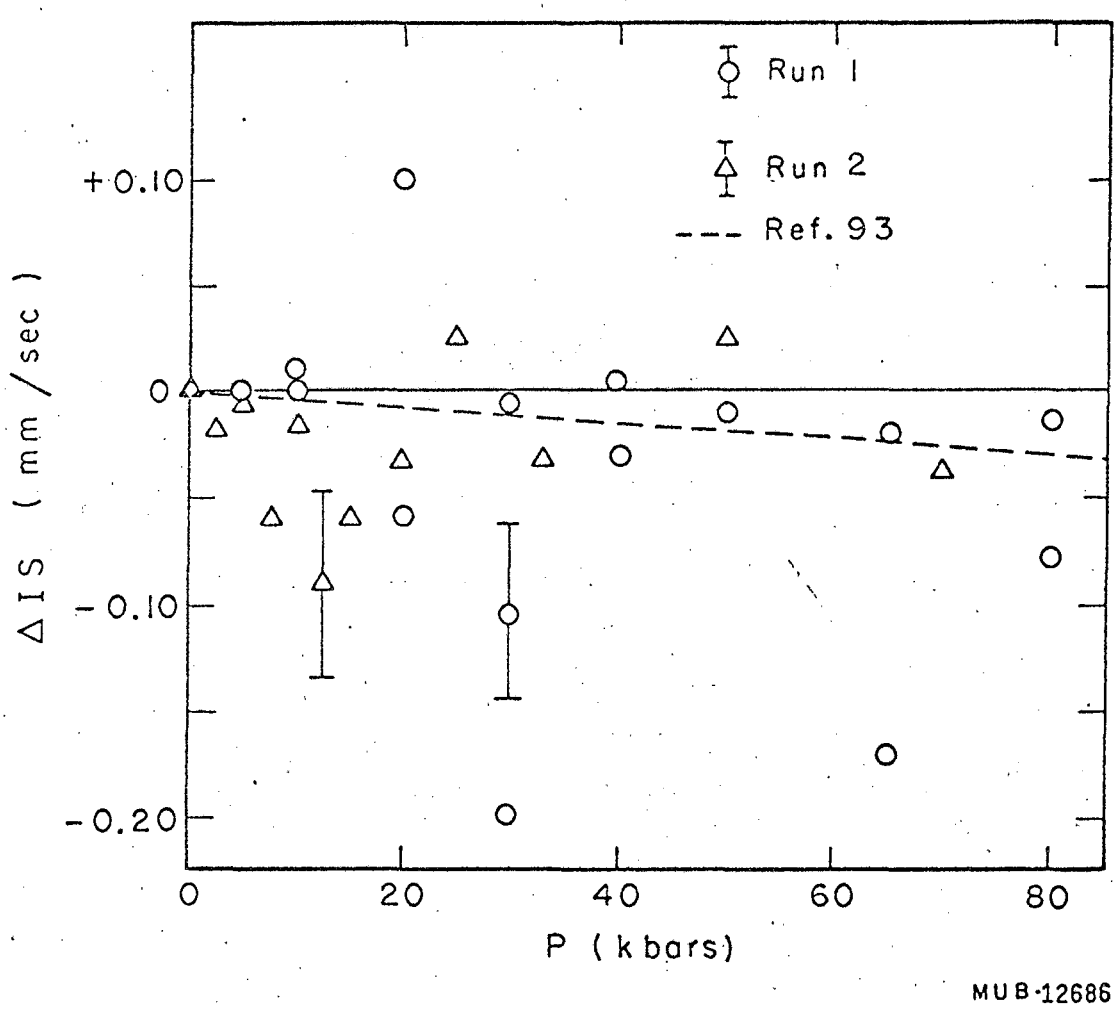

Fig. II-16 Variation of the isomer shift of Fe^{57} in nickel as a function of pressure. Error flags are indicated on single points.

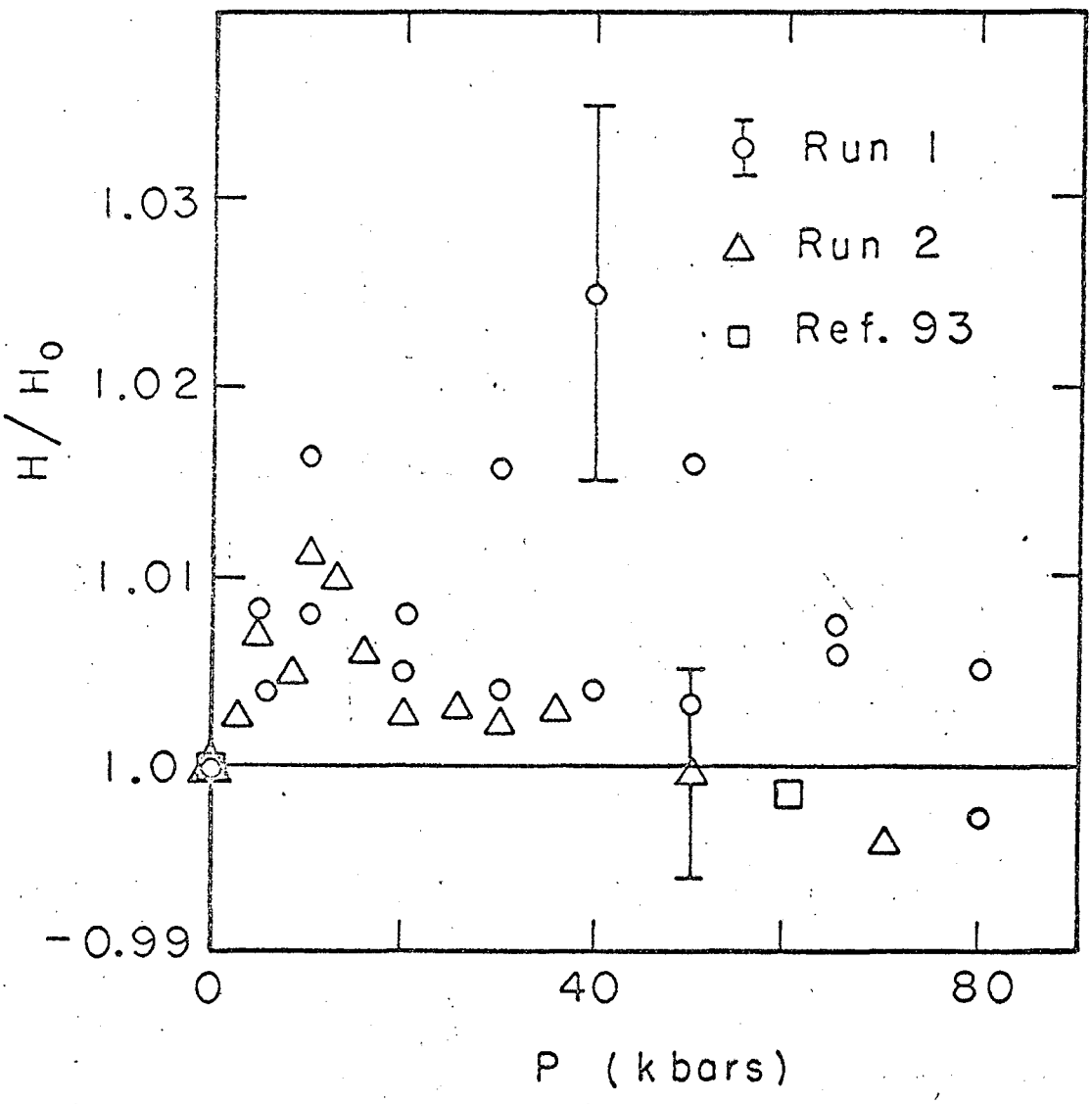

MUB-12681

Fig. II-17 Variation of the internal magnetic field of Fe^{57} in nickel as a function of pressure. Error flags are indicated on single points.

or in terms of the relative volume change by

$$\frac{d(IS)}{d(V/V_o)} = 0.0789 \text{ cm/sec} . \qquad \text{(II-21)}$$

The value of the isomer shift at 1 atmosphere relative to stainless steel is +0.146±.04 mm/sec. It is noted that the pressure variation of the isomer shift for Fe^{57} in nickel is about half the value observed for Fe^{57} in iron, while the compressibilities of iron and nickel are approximately the same magnitude.[91]

3. Discussion

In order to understand the pressure dependence of the isomer shift of Fe^{57} in nickel, it is worthwhile to digress and review the results on Fe^{57} in iron metal. It was mentioned in Sec. II-D that the observed volume variation of the isomer shift of Fe^{57} in iron is attributed to a scaling of the 4s wavefunction with volume. This assumes that the number of conduction electrons remains constant and they are uniformly compressed upon application of pressure. Resistivity-volume data on iron shows that the positive volume derivative of the resistance may be attributed totally to a change in the electron-lattice interaction, consequently, to an increase in the Debye temperature, the number of conduction electrons remaining constant.[103] However, resistivity results on nickel indicate a somewhat smaller decrease in the resistivity with volume than would be expected on the basis of the electron-lattice interaction.[22] The additional resistance may be caused by a decrease in the number of conduction electrons. An estimate of the magnitude of the decrease in conduction electron density is obtained from magnetic data. The saturation moment, σ_o, of nickel decreases with decreasing

volume by an amount given by[104]

$$\frac{d\ln \sigma_o}{d\ln V} = +0.5 \; . \qquad \text{(II-22)}$$

If it is assumed that the decrease in the saturation moment is caused by a transfer of electrons from the conduction band to the unfilled 3d band, the decrease in the conduction electron density is given by

$$\left[\frac{d\ln \psi_{4s}(0)^2}{d\ln V}\right]_{4s \to 3d} = +0.5 \qquad \text{(II-23)}$$

Thus, assuming the remaining conduction electron density to be uniformly compressed, the total change in the conduction electron density with volume is given by the sum of Eqs. (II-16) and (II-23), or

$$\left[\frac{d\ln \psi_{4s}(0)^2}{d\ln V}\right]_{total} = -0.5 \qquad \text{(II-24)}$$

The volume variation of the isomer shift is then given by

$$\frac{d(IS)}{d(V/V_o)} \approx 0.07 \text{ cm/sec.} \qquad \text{(II-25)}$$

This result is in agreement with the experimental result, 0.0789 cm/sec. Considering the assumptions made in this calculation, the agreement with experiment may be fortuitous. In any case, there appears to be a decrease in the 4s electron density which partially counteracts the increase in total s-electron density with compression. The isomer shift does not show any discontinuity at 10 kbars, but this is not surprising. Since the isomer shift is proportional to the total charge density at the nucleus, it is not expected to be affected by small variations in the behavior of the conduction electrons. In addition, the isomer shift

at a second order phase transition is expected to be of the same magnitude as determined for iron at the Curie point, 0.01 mm/sec.[62] This is well beyond the accuracy in the determination of the isomer shift in this work.

The initial increase in the magnitude of the internal field of Fe^{57} in nickel with pressure is in agreement with the increase in the field at Ni^{61} nuclei in nickel.[94] This result further confirms the importance of the host lattice in determining the pressure dependence of the internal field. The pressure dependence of the internal field may be used to estimate the variation of the Curie temperature with pressure.[105] Since the internal field is approximately proportional to the magnetization, the temperature dependence of the field may be estimated by the Bloch $T^{3/2}$, which describes the temperature variation of the magnetization at low temperatures.[74] In terms of the internal magnetic field, this is written

$$H(T)/H(0°K) = 1 - (T/\Theta)^{3/2} \quad T \ll \Theta \qquad \text{(II-26)}$$

where Θ is the Curie temperature. In order to correctly calculate the change in the Curie temperature from this equation, measurements of the pressure dependence of H are required at two different temperatures. Since these measurements are not available in the case of nickel, it is sufficient to approximate the change in the Curie temperature with pressure by the expression

$$\frac{d\ln\Theta}{dP} = \frac{2}{3}\,\frac{d\ln H}{dP} \quad . \qquad \text{(II-27)}$$

Using the reported value of $d\ln H/dP$ for Ni^{61} in nickel[94] given earlier, the calculated increase in the Curie temperature is 0.37°K/kbar compared with the observed value of 0.35°K/kbar.[75] This result indicates the

validity of the above assumptions and illustrates a useful application of high pressure Mössbauer data in solid state physics. The observed peak in the internal field at 10 kbars is unexplainable at this time. Compressibility and resistivity data indicate that the peak is characteristic of nickel and not the Fe^{57}-nickel system. A similar peak is observed at approximately 75 kbars for the internal field at Fe^{57} in cobalt.[93] Also, on the basis of NMR results, Anderson[105] has suggested the possibility of a maximum in the Curie temperature of cobalt. A similar maximum might be observed in nickel on the basis of the present results.

4. Conclusions

The above results illustrate the usefulness of Mössbauer effect studies in understanding the coupling of nuclear parameters to the bulk properties of materials. The techniques applied in this work are easily applicable to other Mössbauer experiments. Several experiments are of direct interest with respect to the above results. First, further measurements of the bulk properties of nickel are required from 1 atmosphere to 20 kbars. These data might answer the question of the origin of the observed anomalies at 10 kbars. Second, Mössbauer measurements of Fe^{57} in cobalt with an emphasis on the low pressure region are required in order to confirm the importance of the host lattice in determining the pressure dependence of the internal field.

ACKNOWLEDGEMENTS

I wish to express my sincere thanks to:

Professor George Jura, for his continued interest and guidance which have made this work possible.

My wife, whose patience and encouragement have been a source of inspiration throughout my graduate career.

Mr. Duane Newhart, who contributed his assistance in several aspects of the experimental work.

And my collegues of the high pressure laboratory, Mr. Walter Stark, Dr. David Phillips, Mr. John Przybylinski, and Mr. James Burton, whose helpful discussions are deeply appreciated.

This work was performed under the auspices of the United States Atomic Energy Commission.

REFERENCES

1. J. C. Jamieson, in Physics of Solids at High Pressures (Academic Press, New York, 1964) p. 444.

2. R. G. McQueen, in Metallurgy at High Pressures and High Temperatures (Gordon and Breach Science Publishers, New York, 1964) p. 44.

3. C. A. Swenson, in Physics of Solids at High Pressures (Academic Press, New York, 1964) p. 548.

4. O. L. Anderson, in Progress in Very High Pressure Research (John Wiley and Sons, Inc., New York, 1961) p. 225.

5. J. S. Dugdale and F. E. Simon, Proc. Roy. Soc., London A218, 291 (1953).

6. Guenter Alers, University of California Radiation Laboratory Report UCRL-10757, January, 1964.

7. Walter Stark and George Jura, University of California Radiation Laboratory Report UCRL-16658, 30 (1965).

8. D. C. Wallace, P. H. Sidles and G. C. Danielson, J. Appl. Phys. 31, 168 (1960).

9. N. Bernardes and C. A. Swenson, in Solids Under Pressure (McGraw-Hill Book Co., New York, 1963) p. 101.

10. E. Grüneisen, in Handbuch der Physik, Vol. 10 (J. Springer, Berlin, 1926) p. 22.

11. T.H.K.Barron, Ann. Phys. 1, 77 (1957).

12. T.H.K. Barron, Phil. Mag. 46, 720 (1955).

13. F. Bloch, Z. Physik 52, 555 (1930).

14. E. Grüneisen, Ann. Physik 16, 530 (1933).

15. J. M. Ziman, Principles of the Theory of Solids (Cambridge University Press, London (1964).

16. J. M. Ziman, in Physics of Solids at High Pressures (Academic Press, New York, 1965) p. 171.

17. C. Matthiessen and P. Vogt, Ann. d. Phys. u. Chem. 122, 19 (1864).

18. J. Bardeen, J. Appl. Phys. 11, 88 (1940).

19. Karl A. Gschneidner, Jr., in Solid State Physics, Vol. 16 (Academic Press, New York, 1964).

20. D. K. C. MacDonald and K. Mendelssohn, Proc. Roy. Soc. London A202, 523 (1950).

21. D. K. C. MacDonald and I. M. Templeton, Phil. Mag. 42, 432 (1951).

22. A. W. Lawson, Prog. in Metal Physics 6, 1 (1956).

23. P. C. Souers and G. Jura, Science 143, 3605, 467 (1964).

24. M. H. Lennsen and A. Michels, Physica 2, 1091 (1935).

25. J. S. Dugdale and D. Gugan, Proc. Roy. Soc., London A241, 397 (1957).

26. William Paul, in High Pressure Physics and Chemistry, Vol. 1 (Academic Press, New York, 1963) p. 299.

27. P. W. Bridgman, Proc. Amer. Acad. Arts. Sci. 81, 4, 165 (1952).

28. P. W. Montgomery, H. Stromberg, G. H. Jura, and G. Jura, in High Pressure Measurement (Butterworth's, Washington, 1963) p. 1.

29. H. Stromberg and G. Jura, Science 138, 1344 (1962).

30. G. Chanin, E. A. Lynton and B. Serin, Phys. Rev. 114, 719 (1959).

31. P. W. Bridgman, Proc. Am. Acad. Arts Sci. 76, 55 (1948).

32. John C. Jamieson, in High Pressure Measurement (Butterworth's, Washington, 1963) p. 389.

33. John M. Walsh and Russel H. Christian, Phys. Rev. 97, 6, 1544 (1955).

34. F. C. Nix and D. MacNair, Phys. Rev. 60, 597 (1941).

35. W. F. Giaque and P. F. Meads, J. Amer. Chem. Soc. 63, 1897 (1941).

36. G. N. Lewis and M. Randall, Thermodynamics (McGraw-Hill Book Co., New York, 1961).

37. S. B. Kormer, A. I. Funtikov, V. D. Urlin and A. N. Kolesnikov, Soviet Phys., JETP 15, 477 (1962).

38. J. C. Slater, Introduction to Chemical Physics (McGraw-Hill Book Co., New York, 1939) p. 452.

39. D. John Pastine, J. Appl. Phys. 35, 11, 3407 (1964).

40. B. F. Figgins, G. O. Jones and D. P. Riley, Phil. Mag. 1, 747 (1956).

41. D. Lazarus, Phys. Rev. 76, 545 (1949).

42. R. E. Schmunk and Charles S. Smith, J. Phys. Chem. Solids 9, 100 (1959).

43. J. C. Slater, Introduction to Chemical Physics (McGraw-Hill Book Co., New York, 1939) Chap. X.

44. R. V. Pound, G. B. Benedek, and R. Drever, Phys. Rev. Letters 7, 405 (1961).

45. M. Nicol and G. Jura, Science 141, 1035 (1963).

46. D. N. Pipkorn, G. K. Edge, P. Debrunner, G. De Pasquali, H. G. Drickamer and H. Frauenfelder, Phys. Rev. 135, A1604 (1964).

47. V. N. Panyushkin and F. F. Voronov, Soviet Physics, JETP Letters 2, 97 (1965).

48. J. A. Stone, M. Nicol, G. Jura and J. O. Rasmussen, University of California Radiation Laboratory Report UCRL-10630 Rev., April 1963.

49. Hans Frauenfelder, The Mössbauer Effect (W. A. Benjamin, Inc., New York, 1962).

50. Gunther K. Wertheim, Mössbauer Effect: Principles and Applications (Academic Press, New York, 1964).

51. R. L. Mössbauer, Z. Physik 151, 124 (1958).

52. D. A. Shirley, M. Kaplan and P. Axel, Phys. Rev. 123, 816 (1961).

53. L. R. Walker, G. K. Wertheim and V. Jaccarino, Phys. Rev. Letters 6, 98 (1961).

54. D. A. Shirley, Rev. Mod. Physics 36, 339 (1964).

55. R. V. Round and G. A. Rebka, Jr., Phys. Rev. Letters 4, 274 (1960).

56. S. S. Hanna, J. Heberle, C. Littlejohn, G. J. Perlow, R. S. Preston and D. H. Vincent, Phys. Rev. Letters 4, 177 (1960).

57. W. Marshall, Phys. Rev. 110, 1280 (1958).

58. R. E. Watson and A. J. Freeman, Phys. Rev. 123, 2027 (1961).

59. P. W. Anderson, Phys. Rev. 124, 41 (1961).

60. P. W. Anderson and A. M. Clogstrom, Bull. Amer. Phys. Soc. 6, 124 (1961).

61. D. E. Nagle, H. Frauenfelder, R. D. Taylor and D. R. Cochran, Phys. Rev. Letters 5, 364 (1960).

62. R. S. Preston, S. S. Hanna and J. Heberle, Phys. Rev. 128, 2207 (1962).

63. R. L. Streever, Jr. and L. H. Bennett, Phys. Rev. 131, 2000 (1963).

64. David H. Anderson and George A. Samara, J. Appl. Phys. 35, 3043 (1964).

65. G. B. Benedek, Magnetic Resonance at High Pressures (Interscience Publishers, Inc., New York, 1963) p. 21.

66. J. G. Dash, B. D. Dunlap and D. G. Howard, Phys. Rev. 141, 376 (1966).

67. Y. Kov, A. Tsujimura and T. Hihara, J. Phys. Soc. Japan 19, 1493 (1964).

68. L. H. Bennett and R. L. Streever, Jr., J. Appl. Phys. 33, 10935 (1962).

69. R. V. Hanks, Phys. Rev. 124, 1319 (1961).

70. Malcon F. Nicol, University of California Radiation Laboratory Report UCRL-10899, August 1963.

71. J. D. Litster and G. B. Benedek, J. Appl. Phys. 34, 688 (1963).

72. Ronald Zane, University of California Radiation Laboratory Report UCRL-16401, September 1965.

73. J. G. Dash, R. D. Taylor, D. E. Nagle, D. P. Craig and W. M. Wisscher, Phys. Rev. 122, 1116 (1961).

74. Charles Kittel, Introduction to Solid State Physics (John Wiley and Sons, Inc., New York, 1956).

75. L. Patrick, Phys. Rev. 93, 384 (1954).

76. Larry Kaufman, E. V. Clougherty and R. J. Weiss, Acta Met. 11, 323 (1963).

77. D. Bancroft, E. L. Peterson and S. Minshall, J. Appl. Phys. 27, 557 (1956).

78. P. C. Johnson, B. A. Stein and R. S. Davis, J. Apply. Phys. 33, 557 (1962).

79. H. G. Drickamer and A. I. Balchan, Rev. Sci. Instr. 32, 308 (1961).

80. W. Stark and G. Jura, University of California Radiation Laboratory UCRL-11592 (1965).

81. Walter F. Claussen, Rev. Sci. Instr. 31, 878 (1960).

82. L. Kaufman, A. Leyenaar and J. S. Harvey, in Progress in Very High Pressure Research (John Wiley and Sons, New York, 1961) p. 89.

83. J. E. Hilliard, ASME Paper No. 60-WA-271, New York (1960).

84. G. C. Kennedy and R. C. Newton, in Solids Under Pressure (McGraw-Hill Book Co., New York, 1962) p. 163.

85. J. C. Jamieson and A. W. Lawson, J. Appl. Phys. 33, 776 (1962).

86. R. L. Clendenen and H. G. Drickamer, J. Phys. Chem. Solids 25, 865 (1964).

87. A. M. Clogstron and V. Jaccarino, Bull. Am. Phys. Soc. 8, 249 (1963).

88. G. K. Wertheim, J. Appl. Phys. 32, 1105 (1961).

89. V. I. Gol'danski, The Mössbauer Effect and Its Applications in Chemistry, (Consultants Bureau, New York, 1964) p. 57.

90. J. E. Hilliard and J. W. Cahn, in Progress in Very High Pressure Research (John Wiley and Sons, New York, 1961) p. 109.

91. P. W. Bridgman, Proc. Amer. Acad. Arts Sci. 77, 187 (1949).

92. T. Mitsui, in Physics of Solids at High Pressures (Academic Press, New York, 1964) p. 213.

93. H. G. Drickamer, R. L. Ingalls and C. J. Coston, in Physics of Solids at High Pressures (Academic Press, New York, 1964) p. 313.

94. L. H. Bennett, J. Appl. Phys. 36, 9425 (1965).

95. F. E. Obenshain and H. H. F. Wegener, Rev. Mod. Phys. 36, 408 (1964).

96. G. K. Wertheim, Phys. Rev. Letters 4, 403 (1960).

97. V. Arp, D. Edmonds and R. Petersen, Phys. Rev. Letters 3, 212 (1959).

98. A. C. Gossard and A. M. Portis, Phys. Rev. Letters 3, 164 (1959).

99. Lawrence H. Bennett and Ralph L. Streever, Jr., J. Appl. Phys. 33, 1093 (1962).

100. Ralph L. Streever, Jr., Phys. Rev. Letters 10, 232 (1963).

101. A. J. F. Boyle, D. St. P. Bunbury, and C. Edwards, Phys. Rev. Letters 5, 553 (1960).

102. T. Kushida, A. H. Siever, V. Koi, and A. Tsujimura, J. Appl. Phys. Suppl. 33, 1079 (1962).

103. John C. Jamieson, in Third Annual Report to ONR on High Pressure Research, Chicago (1959) p. 31.

104. D. Bloch and R. Pauthenet, J. Appl. Phys. 36, 1229 (1965).

105. D. H. Anderson, Bull. Am. Phys. Soc. 10, 75 (1965).

This report was prepared as an account of Government sponsored work. Neither the United States, nor the Commission, nor any person acting on behalf of the Commission:

A. Makes any warranty or representation, expressed or implied, with respect to the accuracy, completeness, or usefulness of the information contained in this report, or that the use of any information, apparatus, method, or process disclosed in this report may not infringe privately owned rights; or

B. Assumes any liabilities with respect to the use of, or for damages resulting from the use of any information, apparatus, method, or process disclosed in this report.

As used in the above, "person acting on behalf of the Commission" includes any employee or contractor of the Commission, or employee of such contractor, to the extent that such employee or contractor of the Commission, or employee of such contractor prepares, disseminates, or provides access to, any information pursuant to his employment or contract with the Commission, or his employment with such contractor.